

Simulations of global hurricane climatology, interannual variability, and response to global warming using a 50km resolution GCM

Ming Zhao^{1,2}, Isaac M. Held², Shian-Jiann Lin² and Gabriel A. Vecchi²

¹University Corporation for Atmospheric Research

²Geophysical Fluid Dynamics Laboratory / NOAA, Princeton, New Jersey, USA

Submitted (01/23/09), Revised (06/01/09), Journal of Climate

Corresponding author address:

Dr. Ming Zhao

Geophysical Fluid Dynamics Laboratory / NOAA

Princeton University Forrestal Campus / US Route 1

P.O.Box 308 Princeton

New Jersey 08542

Abstract.

A global atmospheric model with roughly 50 km horizontal grid spacing is used to simulate the interannual variability of tropical cyclones using observed sea surface temperatures (SSTs) as the lower boundary condition. The model's convective parameterization is based on a closure for shallow convection, with much of the deep convection allowed to occur on resolved scales. Four realizations of the period 1981-2005 are generated. The correlation of yearly Atlantic hurricane counts with observations is greater than 0.8 when the model is averaged over the four realizations, supporting the view that the random part of this annual Atlantic hurricane frequency (the part not predictable given the SSTs) is relatively small (< 2 hurricanes/yr). Correlations with observations are lower in the East, West and South Pacific (roughly 0.6, 0.5 and 0.3) and insignificant in the Indian ocean. The model trends in Northern Hemisphere basin-wide frequency are consistent with the observed trends in the IBTrACS database. The model generates an upward trend of hurricane frequency in the Atlantic and downward trends in the East and West Pacific over this time frame. The model produces a negative trend in the Southern Hemisphere that is larger than that in the IBTrACS.

The same model is used to simulate the response to the SST anomalies generated by coupled models in the CMIP3 archive, using the late 21st century in the A1B scenario. Results are presented for SST anomalies computed by averaging over 18 CMIP3 models and from individual realizations from three models. A modest reduction of global and Southern Hemisphere hurricane frequency is obtained in each case, but the results in individual Northern Hemisphere basins differ among the models. The vertical shear in the Atlantic Main Development Region (MDR) and the difference between the MDR SST and the tropical mean SST are well correlated with the model's Atlantic storm frequency, both for interannual variability and for the intermodel spread in global warming projections.

1. Introduction

As global atmospheric climate models move to finer horizontal resolution, the hope is that simulations of the climatology of tropical storms will improve to the point that they can be used to reliably study the impact of changing climate conditions (including global warming) on storm statistics. Recent encouraging results with global models include atmosphere-only simulations (e.g., Bengtsson et al. 2007a b; Oouchi et al. 2006; LaRow et al. 2008) and coupled models (Vitart 2006; Gualdi et al. 2008). These studies suggest that atmospheric resolutions in the range of 20-100km may be sufficient to study many aspects of genesis and storm distribution. Recent simulations with an 18km regional climate model over the North Atlantic (Knutson et al. 2007) (below K07) are also encouraging with regard to the quality of the simulation of interannual variability of hurricane frequency obtainable at the lower end of this meso- β range of resolutions, even though simulations of intensity remain inadequate. The hope is that simulations of storm frequency and intensity are effectively decoupled, so that reliable simulations of frequency can be generated in models with an unrealistic distribution of intensities. Until much higher resolution climate models become available, the considerable promise of predictions of tropical storm frequency over seasonal to decadal time scale using dynamical models (e.g., Vitart 2006; Vitart et al. 2007) will be dependent on this decoupling of frequencies from intensities,

The standard version of the AM2.1 atmospheric model developed at the Geophysical Fluid Dynamics Laboratory (Anderson et al. 2004) has a horizontal grid spacing of 2 degrees latitude by 2.5 degrees longitude. We present results here from a version of AM2.1 with roughly 0.5 degree (\sim 50km) grid spacing, with modified sub-grid closures. The moist physics has been modified because the standard AM2 choice results in too quiescent a tropics, with Atlantic storminess particularly suppressed, even as one moves to higher resolution. We have also been motivated to try to simplify the moist convective and cloud closures in the model to facilitate studies of the parameter dependence of our results and because we feel that simpler, less intrusive schemes become more justifiable as resolution increases. We evaluate the quality of the model's tropical storm statistics by running over observed sea surface temperatures (SSTs) from the 1981-2005

period. We then examine the sensitivity of this model to the increase in SSTs projected by several coupled climate models over the 21st century.

It is important that a model utilized to project tropical storm statistics into the future be capable of simulating observed trends in storm frequency. The well-documented upward trend in the North Atlantic over the past 25 years is well simulated by the regional model analyzed in K07, which is relaxed towards the National Centers for Environmental Prediction (NCEP)-National Center for Atmospheric Research (NCAR) reanalysis (Kalnay et al. 1996) on large scales. In this reanalysis, there is a trend towards destabilization of the atmosphere over the Atlantic, and elsewhere in the tropics, raising the question of whether this destabilization, the reality of which has been questioned (Santer et al. 2008), is responsible for a substantial part of the trend in hurricane counts in that model (Garner et al. 2009). The model under consideration here does not, on average, produce a destabilization of the mean tropical lapse rate as the ocean temperatures warm due to increasing greenhouse gases. It is of interest whether such a model can simulate the observed positive Atlantic trends, while simultaneously simulating the observed absence of a trend or negative trends in other basins. The recent simulation of LaRow et al. (2008) suggests that global models are capable of simulating the Atlantic trend with SST information alone.

With regard to future projections, a key question is whether or not the details of the SST projections are important for the simulated changes in tropical storm statistics, or if at least some aspects of these changes are robust to these differences. Emanuel et al. (2008) suggests considerable sensitivity to differences among the World Climate Research Program Coupled Model Intercomparison Project 3 (CMIP3) model projections, as does continuing work with the K07 Atlantic regional model (Knutson et al. 2008, J. Sirutis, personal communication). We are limited by the computational expense in how extensive an exploration of these sensitivities we can perform, but as a start along these lines we compare results obtained with a multi-model mean projection for SSTs with projections from three individual models using trends from the Intergovernmental Panel on Climate Change (IPCC) A1B SRES emissions scenario similar to those used in Knutson et al. (2008).

Running atmospheric models over observed SSTs has significant limitations in the context of tropical storm simulations. As is well-known (e.g., [Bender et al. 1993](#); [Schade and Emanuel 1999](#)), fixing SSTs can distort storm intensities, especially for strong slow moving storms. The extent to which a decoupled atmospheric model, given SSTs, should be able to accurately simulate the climatology of genesis is also uncertain. Experience with global models to date is encouraging, yet the evidence that decoupling can distort intra-seasonal variability (e.g., [Waliser et al. 1999](#)), and monsoonal responses to global warming ([Douville 2005](#)) suggests that there is some concern here as well. Keeping these limitations in mind, the value of uncoupled models in our view is best determined by the quality of the simulations of interannual variability and trends obtained.

We first describe the model formulation in Section 2, including a summary of the global simulation and a brief discussion of the method used to optimize the convective closure. Section 3 contains a description of the tropical storm climatology in the model and an ensemble of four simulations of the 1981-2005 period with observed SSTs. Simulations using future projections of SSTs are provided in Section 4. Section 5 provides discussion and conclusions.

2. Model Formulation and climate simulation

If one increases the horizontal resolution in AM2.1 the climate simulation improves in a number of respects. A model of this type, at 50km resolution, has been used to generate a time-slice climate change simulation coordinated with the ongoing North American Climate Change and Assessment Program (<http://www.narccap.ucar.edu/>). This model has also been used to study regional structures in the Asian monsoon system ([Lau and Ploshay 2009](#)). But the tropical storm climatology generated by the model remains deficient at this higher resolution. In particular, the Atlantic is too quiescent.

To improve this aspect of the model, for this and for related projects at relatively high resolutions, we have made the following changes to AM2.1: the finite-volume dynamical core ([Lin 2004](#)) on a latitude-longitude grid has been replaced by a finite-volume core using a cubed-sphere grid topology ([Putman and Lin 2007](#)); the number of vertical levels has been increased from

24 to 32; the prognostic cloud fraction scheme has been replaced by a simpler diagnostic scheme assuming a sub-grid scale distribution of total water; and the relaxed Arakawa-Schubert convective closure in AM2 has been replaced by a scheme based on the parameterization of shallow convection by [Bretherton et al. \(2004\)](#). The model retains the surface flux, boundary layer, land surface, gravity wave drag, large-scale cloud microphysics, and radiative transfer modules from AM2 ([Anderson et al. 2004](#)). We refer to this model development branch as HIRAM2 (High Resolution AM2) , and the specific version described here as the C180HIRAM2.1 . The notation C180 indicates 180×180 grid points in each face of the cube; the size of the model grid varies from 43.5 km to 61.6 km.

The gnomonic projection in the cubed-sphere geometry described by [Putman and Lin \(2007\)](#), compared to other options with the cubed-sphere topology, is chosen due to its overall accuracy and excellent grid uniformity . Compared to a latitude-longitude grid, the use of the cubed-sphere grid in the finite-volume core eliminates the need for the “flux-form semi-Lagrangian” extension for the transport processes ([Lin and Rood 1996](#)) and the polar Fourier filtering for the fast waves, resulting in improved computation and communication load balance, using 2D domain decomposition on each of the six faces of the cube. This new dynamical core greatly improves the model’s scalability when using large numbers of processors.

Most of the extra vertical resolution as compared with AM2.1 is placed near the tropopause. The low AM2 resolution in that region has been found to be a significant liability to several aspects of the simulation, including stratospheric water and polar surface pressures, but more significantly for this study the extra resolution near the tropical tropopause should better represent the sensitivity of storms to upper tropospheric conditions.

The use of a diagnostic cloud fraction scheme is motivated in large part by efficiency, a significant consideration as one moves to higher resolution; short integrations suggest that the effect of this simplification on the aspects of the simulation on which we focus here is minor. The approach used in AM2 ([Tiedtke 1993](#)), in which cloud fraction is a prognostic variable, is replaced with a simpler assumption concerning the PDF of total water (S. Klein, personal

communication). A description of this parameterization is provided in Appendix A.

The convective closure of [Bretherton et al. \(2004\)](#) assumes a single strongly entraining and detraining plume, with entrainment/detrainment profiles determined by a parcel buoyancy sorting algorithm that is a simplification of that used by [Kain and Fritsch \(1990\)](#), including a plume vertical momentum equation and a parameterization of cloud top penetrative entrainment of air between the level of neutral buoyancy and the maximum vertical extent of the plume. The base mass flux in the plume is determined by estimates of the boundary layer eddy kinetic energy and of the convective inhibition. Although strongly entraining, the plume can provide deep convection when the atmosphere is sufficiently moist to limit the loss of buoyancy due to the entrainment. But deep convection is sufficiently inhibited that a substantial fraction of the rainfall in the tropics (30% for C48 resolution, 38% for C180 resolution) occurs through the large-scale (stratiform) cloud module rather than through the convection module, a larger fraction than in AM2.1 (7.5% for C48 resolution). Our modifications to the [Bretherton et al. \(2004\)](#) scheme are also described in appendix A.

Our choice of a shallow convection scheme, based on a strongly entraining plume model, on which to base the convective closure is motivated by the desire for a scheme that is minimally intrusive, allowing the large-scale to do much of the work. Our intuition is that the distortions that result become acceptable for some purposes as one moves to mesoscale resolutions. As an important example, since convection in the eye-wall of a mature storm is slanted rather than vertical, typical upright convective parameterizations have the potential to distort the amphitheater-like inner structure of a tropical storm. Although this issue is likely to be more relevant at finer resolutions than utilized here, our experience is that it can be beneficial for large-scale condensation to play a significant role throughout the tropics as well as dominate near the storm center even at this relatively low mesoscale resolution.

The overall convective entrainment rate is adjusted so as to maintain a cloud field over the oceans that produces a reasonable energy balance at the top of the atmosphere. However, when integrated at lower (C48) resolution especially, this model severely underestimates the

precipitation over tropical land areas, especially the Amazon. The deficiency slowly disappears as one moves to higher resolution, but is still evident in the C180 model. Decreasing entrainment rates over land improves the model in this respect, as illustrated in Fig. 1. Similar results on the effect of entrainment rate over land are also found by [Park and Bretherton \(2009\)](#) using the NCAR Community Atmosphere Model (CAM). The diurnal cycle of rainfall over the Amazon (not shown) is distorted by this procedure, in that there is too strong a maximum in rainfall in mid-afternoon. We feel that it is important to have a high quality simulation of the seasonal cycle of tropical winds in this type of study, in order to create the appropriate environments for tropical storm genesis, and have chosen this modification, despite its arbitrary character, so as to improve this large-scale seasonal mean flow. The land/ocean entrainment difference in the C180 model is small in any case (see Appendix A); this aspect of the model design is of more relevance to the C90 (100km) version of this model, results of which will be described elsewhere.

As a rough indication of the quality of the model's climate simulation, we choose a small number of global fields (precipitation, 850 and 200 hPa zonal winds, and surface pressure) and compute the rms departure from observations, comparing C48, C90, and C180 versions of HIRAM2.1 with AM2.1 and with 10 other models for which prescribed SST simulations are available in the CMIP3 data base. For each variable, we normalize the rms error by the observed standard deviation of spatial variation of the time-mean fields – over the period 1979-1996 for the Climate Prediction Center Merged Analysis of Precipitation (CMAP, [Xie and Arkin 1996](#)) data and 1958-1997 for NCEP-NCAR re-analysis ([Kalnay et al. 1996](#)). We show the statistics for the annual global mean and the Aug-Sept-Oct (ASO) mean over 0-30N, the latter being of special relevance to the Atlantic storm season. We find in Fig. 2 that the relatively good simulation provided by AM2.1, among other models in this database, is maintained and in fact improved significantly as we move to the C180HIRAM simulation. The precipitation figures should be viewed with some skepticism in that there is dependence on the choice of dataset and on the smoothing/interpolation algorithm needed to compare data and models. The surface pressure and zonal wind statistics are more robust, and for these statistics the performance of both the C180 and

C90 models is superior to the (mostly lower resolution) models in the CMIP3 database. Among these statistics, the improvement from C90 to C180 is especially notable in the tropical 850 hPa flow. The trade winds are too strong in this model at low resolution; the upper tropospheric eddy momentum fluxes decrease with increasing resolution, reducing the strength of the trade winds to more realistic values.

While we have not performed a complete sensitivity analysis of the relative importance of the various changes to AM2.1, it is evident that the change in convection scheme, with more inhibited deep convection, is essential for the quality of the storm simulation described below. In addition to allowing more intense storms to form, the increased horizontal resolution, along with the increased vertical resolution, also improves the simulation by improving the large-scale flow.

3. Tropical storm climatology, interannual variability and decadal trends

We have completed four simulations of the 1981-2005 period with this C180 model. The simulations follow broadly the setup for the Atmospheric Model Intercomparison Project (AMIP) and are referred to as AMIP runs below. In these simulations, in addition to the SSTs specified from UK Met Office HadISST 1.1 (Rayner et al. 2003), the well-mixed greenhouse gases and both tropospheric and stratospheric ozone vary from year to year, following the procedure used in the CM2.1 historical simulations in the CMIP3 database (Delworth et al. 2006). We have chosen in these initial simulations to eliminate all variations in anthropogenic and volcanic aerosols. In retrospect it might have been preferable to exclude the greenhouse gas and ozone variations as well, but experiments with the C90 100km version suggest that the changes in the well-mixed greenhouse gases and ozone are not playing a significant role in these prescribed-SST simulations.

We continue by describing the tropical storm climatology in the C180 model. To compare with the global hurricane observations, we use the data from the International Best Track Archive for Climate Stewardship (IBTrACS), available on-line through <http://www.ncdc.noaa.gov/oa/ibtracs/>. We refer to Kruk et al. (2008) for a description of this dataset. The IBTrACS provides estimates for both 10-min and 1-min maximum

sustained wind. We use 1-min wind since it is used in NOAA's Hurricane Research Division dataset (HURDAT, <http://www.aoml.noaa.gov/hrd/hurdat/>) and we would like to have the observed North Atlantic hurricanes match exactly those in the HURDAT dataset. We follow the definition of the ocean basins and naming conventions used in the IBTrACS. A storm is assigned to an ocean basin based on its genesis location.

The algorithm we use for detecting and tracking model storms is adapted from the earlier work by Knutson et al. (2007) and Vitart et al. (1997 2003) with small simplifications/modifications described in Appendix B. Appendix B also discusses some sensitivities of storm counts to the parameters used in the algorithm as well as the justifications for our choice of the parameters. For the reasons described in this Appendix, we restrict discussion in this paper for the most part to storms of hurricane strength (i.e., tropical storms with maximum surface wind speed exceeds 33 m s^{-1}). Similar to observations, roughly 50% of identified tropical storms are rejected by the 33 m s^{-1} maximum wind speed threshold for hurricanes. We refer to these hurricane strength storms as “hurricanes” in all ocean basins.

The tracks of all hurricanes in one of our simulations are shown in Fig. 3b, where they are compared with the observations (Fig. 3a) from the IBTrACS. The total number of hurricanes summed over various ocean basins is indicated in Fig. 4, where the results from each of the 4 realizations are provided. In Fig. 5, the seasonal cycle in each of these regions, averaged over the 4 realizations, is compared with observations.

While the number of storms in the North Atlantic is close to that observed, there is on-average a 20% underprediction of hurricanes in the East Pacific and a more significant (40%) overprediction of hurricanes in the West and South Pacific. The over-prediction of the ratio of West Pacific to Atlantic storms is a property of some other global models of this resolution (e.g., Bengtsson et al. 2007a). In the east Pacific hurricanes are often of much smaller scale than in the other basins and the model's under-prediction is likely a reflection of the difficulty in simulating small strong storms with a model of this resolution. In the South Indian Ocean, there is a 17% underprediction of hurricanes. The small numbers in the North Indian Ocean are broadly

consistent with the observations. There are a few model hurricanes in the South Atlantic, where only one hurricane is present in the IBTrACS database over this time period.

The seasonal cycle of the storm counts in the Atlantic is also realistic. It is not always the case that models that generate the correct number of Atlantic storms also produce accurate seasonal cycles (e.g., [LaRow et al. 2008](#)). The overprediction in the West Pacific is most pronounced in May-June, while the underprediction in the East Pacific is largest in Aug-Sept. Over the Northern Indian ocean, the bimodal seasonal distribution with maxima in the spring and fall (owing, presumably, to the suppression of cyclones by shear in the peak monsoon months), is well captured,

If the convective entrainment rate over the oceans is increased in this model, the storm count increases. If no other parameters are changed, an increase in this entrainment rate results in an unrealistic increase in low level clouds over the ocean and in the planetary albedo. Our selection of an entrainment rate was originally based on the need to simulate a realistic planetary albedo; perhaps fortuitously, this setting generates a realistic number of tropical storms, albeit with some overestimation in the West and South Pacific.

A significant deficiency, not unexpected in a model of this resolution, can be seen in the PDF of storm intensity displayed in [Fig. 6](#). Very few storms exceed a wind speed of 50 m s^{-1} , with an unrealistically strong peak in frequency near 30 m s^{-1} . Model storms resemble each other much more than do observed storms. The unrealistic aspects of this PDF discourage us from taking the response of storm intensity to global warming in this model at face value. Yet some of the most basic differences in intensity distributions between basins are captured qualitatively, particularly the more intense storms in the West Pacific as compared to the Atlantic. Preliminary studies suggest that one can increase the average storm intensity, without changing the average storm frequency, by modifying the surface flux formulation so as to change the ratio of the drag coefficients for momentum and water vapor fluxes, as anticipated from the theory of [Emanuel \(1988\)](#). Whether or not it is desirable to generate very strong storms in a 50km model is unclear, given that many strong storms have radii of maximum winds that should not be resolved with a

50km grid.

The model shows significant skill in reproducing the observed year-to-year variability in the North Atlantic, the East and West Pacific and to a lesser degree the South Pacific. Because the total numbers of hurricanes in some basins are significantly different from the observations (Fig. 4), below we show the results of normalizing in each basin by a time-independent multiplicative factor (roughly 1.17, 1.25, 0.71 for the North Atlantic, the East and West Pacific respectively) so as to reproduce the observed number. Fig. 7 shows that the model does an excellent job of simulating the year to year variations in hurricane frequency in the North Atlantic. The correlations for the individual runs of the model with observations are 0.7, 0.78, 0.68, and 0.55. The standard deviation across the model ensemble, computed for each year and then averaged over all years, is 1.7 hurricanes/yr. [Garner et al. \(2009\)](#) obtained a very similar estimate in the regional model utilized by K07, forced not only by the year-to-year variations in SST but also by relaxation of the largest scales in their regional domain towards observations. One would anticipate more variability in a global model in which the large-scale flow is unconstrained than in the regional model used by [Garner et al. \(2009\)](#). If both of these estimates are accurate, the implication would be that the large scale flow variability that is independent of SSTs generates relatively little of the variance in simulations of seasonal storm activity as compared to the noise resulting from small scales.

The correlation of observed Atlantic hurricane counts with the ensemble mean of these four realizations is 0.83 . This value is somewhat higher than one would expect given the correlations with the individual realizations. This expectation is based on the hypothesis of a perfect model that responds exactly as does nature to changes in SSTs and the assumption that the observations have the same (1.7 hurricane) noise level as the model, with Gaussian statistics. In this case, the correlation of the mean of a 4-member ensemble with another realization has only a 20% chance of being as high as 0.83. It is reasonable to conclude that the rms of the observed noise, so defined, is unlikely to be much larger than 1.7 and could be smaller. In any case, it is clear that the number of hurricanes per year in the Atlantic has a large component that is predictable from

SSTs, consistent with the dynamical modeling results of Vitart (2006) and LaRow et al. (2008), as well as a variety of statistical studies.

There is a significant correlation between the spread across the ensemble in each year and the number of storms; in particular the correlation between the standard deviation σ and the mean hurricane count n for each year is 0.53 ($p=0.006$) with a linear regression fit of $\sigma=0.5+0.2n$ for the North Atlantic. The active years 1995 and 2005 have indeed a relatively large spread in the ensemble, but 4 realizations is insufficient to determine in detail how the spread varies from year to year. For example, in 2005, the 4 realizations produce hurricane counts of 13, 12, 8, 15, to which we can compare the observed number of 15, so the spread is strongly affected by one low hurricane year. The Atlantic hurricane tracks for each realization of 2005 are also shown in Fig. 8 to provide the reader with some flavor for the noise level in the model. The year in which the model does most poorly is 1996. (Additional experiments for this particular year are consistent with the hypothesis that this relatively large model-observation difference is significant.) It is of interest to see if there is some aspect of the large-scale atmospheric flow over the tropical Atlantic in 1996 that the model does not simulate well, but we do not pursue this issue here.

Each of the realizations of the model produces a positive linear, least-square trend in Atlantic hurricanes over this period, with the ensemble mean trend being 0.17 hurricane/yr after normalization, compared to the observed trend of 0.22 hurricanes/yr. As shown below (Fig. 11b), the difference between the ensemble mean trend and the observation is not significant, with the observed trend resting within the spread of model trends from the four realizations.

Fig. 9 shows the result for the East Pacific. The model captures reasonably well the less active years of 1988-1989, 1995 and 1998-1999 and the active period of the early 1990s. The model does poorly for the years of 1985, 1994, 2000 and 2002. Overall, the correlation between the ensemble mean and the observation is 0.62 ($r^2 = 0.38$, $p=0.001$, assuming the 25 individual years are temporally independent samples). The model also simulates a downward trend (-0.14/yr) of hurricane frequency in the East Pacific over this time period, compared to the observed trend (-0.24/yr). Detrended, the correlation with the ensemble mean model drops to 0.57. The

correlation between hurricane counts in the East Pacific and West Atlantic in the observations is -0.49, while the model generates correlations ranging from -0.40 to -0.74 in the four realizations, with a correlation of -0.79 between the ensemble means in the two basins.

Fig. 10 shows the corresponding results for the West Pacific. Despite the overestimate of the total West Pacific hurricane number (see Fig. 4), the storm variability is comparable in model and observations after the normalization. The anomalously quiet years of 1983, 1988, 1992 and 1998 are captured well. The poorest simulations appear to be for 1995 and 1999, for which there is roughly a factor of two overestimate in the storm count after normalization. The correlation of the ensemble mean with the observations is 0.52 ($r^2 = 0.28$, $p = 0.007$). The ensemble mean model simulates a downward trend (-0.07/yr) in hurricane frequency over this time period, again close to the observed trend (-0.06/yr).

Fig. 11 provides a summary plot to show the noise level of model simulated correlations and trends for each basin. Fig. 11a displays the correlation of observed hurricane count to the four-member ensemble mean and the correlation of each ensemble member to the ensemble mean of the remaining three. In general, the model means are correlated as well to observations as the model means are to another ensemble member. In the South Pacific there is a correlation of roughly 0.3 between the observed and modeled time series of hurricane count for the 4-member ensemble mean. The model produces no significant correlation in either the North or South Indian ocean. In those regions in which the correlation of the model ensemble mean to observations is low, the correlation of the model ensemble mean to individual realization is also low. Fig. 11b shows the observed and modeled linear trends in hurricane frequency for the period 1981-2005 in each basin. Model trends are calculated from the normalized time series for the ensemble mean and each individual realization. We see fairly large spread in the modeled trends for all basins except, coincidentally perhaps, for the North Indian. The observed trends are generally within the model spread for all basins except for the Indian Ocean - though even there they are quite close.

The model's raw global hurricane count has a downward trend of 0.19 hurricanes/yr, which is contributed from the East (-0.11/yr), West (-0.09/yr), and South Pacific (-0.07/yr) as well

as the South Indian ocean(-0.06/yr). There is no significant trend in the North Indian ocean. The North Atlantic is the only basin in which the model trend over this period is positive (+0.14/yr). If we normalize each basin by the mean observed count, the global trend is reduced to -0.15 hurricanes/yr, since the Pacific basins are then less dominant. This figure corresponds to a reduction of 8% over this 25 year period. This magnitude of the downward trend in the ensemble-mean is larger than the observed global hurricane trend (-0.06 hurricane/yr or -3%) over this period in the IBTrACS dataset; however, the observed trend is contained within the spread of the ensemble members. Roughly 60% of the modeled downward trend comes from the Southern Hemisphere (-0.12 hurricanes/yr) while the observed hurricane trend in the Southern Hemisphere is negligible (-0.01/yr). However, when we take into account all Southern Hemisphere tropical storms (wind speed $> 17 \text{ m s}^{-1}$), we find a much larger downward trend for this period in IBTrACS dataset (-0.12 /yr), close to the model trend in tropical storms of the Southern Hemisphere.

4. Global warming projections

To explore potential changes in hurricane frequency from anthropogenic climate change, we perturb this model with SST anomalies taken from various models of the climate near the end of the 21st century. We consider four anomaly patterns, those obtained from the three models GFDL's CM2.1, the UKMO's HADCM3, and MPI's ECHAM5, and that obtained by taking the ensemble mean for the simulations for 18 models. All results are taken from the A1B simulation in the CMIP3 archive (<https://esg.llnl.gov:8443/index.jsp>) (Meehl et al. 2007) utilized extensively by the IPCC AR4 assessments. We compute the multi-model ensemble mean SST anomaly by differencing the period 2081-2100 and the period 2001-2020 from the historical simulations (labeled 20C3M) in the CMIP3 archive. For each of the three individual models, we use one realization (run 1 in the CMIP3 archive) to compute the 2001-2100 linear trend. The linear trend is then multiplied by 0.8 so that it is consistent in magnitude with the period used for the multi-model ensemble mean. The SST anomalies are computed separately for each month at

each grid point. Fig. 12 shows the mean SST anomalies for the ASO season. Note, for example, that the HADCM3 anomaly is relatively large in the Pacific and relatively small in the Atlantic while ECHAM5 has the largest average anomalies over the ocean domain (40S-40N). We increase the CO_2 in the model atmosphere to a value consistent with the A1B scenario for the period in question. We do not modify the sea ice extent for simplicity, assuming that, with prescribed SSTs, sea ice perturbations have little influence on the tropical climates of interest here.

One possible methodology is to add these SST anomalies to the time-varying SSTs for the period modeled in the previous section. To try to simplify the analysis and save computational resources, we have instead chosen to generate simulations prescribing climatological-SSTs – seasonally varying SSTs with no interannual variability. By perturbing this climatology with the various seasonally-varying but otherwise time-invariant anomalies, the hope is to generate more stable statistics, without the possible complication that the response might depend on the phase of ENSO, for example. Each of these climatological and perturbed runs is of 10 years length.

An unforeseen discovery in generating the climatological storm simulations was that the climatological solutions in the Atlantic were quite sensitive to the choice of climatology. Our initial experiments utilized for the control the climatological SST calculated from an average over 1982-2000 using the NOAA Optimum Interpolation SST Analysis data set (Reynolds et al. 2002). This simulation produces fewer storms in the Atlantic than the time mean of simulations described in the previous section which utilized the UKMO HadISST dataset (3.5/year as compared with 5.5/year). In searching for the reason, we generated an additional climatological simulation with the time average (1982-2005) of the HadISST data and find the number of Atlantic storms to be roughly 5/year, similar to the mean of the time-varying simulations. For this reason, we have carried out two sets of climate change experiments with the same set of SST anomalies but two different control climatological-SSTs.

The response of storm frequency for each of the 4 perturbations based on 2 different climatological-SSTs is shown in Fig. 13 and Fig. 17. We show the fractional changes in hurricane count per year for various ocean basins. Focusing first on the North Atlantic (Fig. 13), we

find that SSTs from two models (CM2.1 and ECHAM5) tend to show an increase in hurricane frequency, while SSTs from HADCM3 and the ensemble mean show a reduction. If we count all tropical storms identified by the algorithm described in Appendix B, the increases in the CM2.1 and ECHAM5 SSTs models are much smaller or close to zero (see Fig. 13, right panel), indicating some of the increase in hurricanes in these models is due to a shift to more intense storms. For the ensemble mean SST anomaly, the reduction of tropical storm and hurricane frequency are respectively $-38\% \pm 25\%$ and $-28\% \pm 15\%$, roughly consistent with the -27% (tropical storms) and -18% (hurricanes) reduction obtained from Knutson et al. (2008) although the latter restricted their study to the Aug-Sept-Oct season only.

The model using the HADCM3 SST anomaly generates an especially large reduction in Atlantic storms. This distinction is also clear if we simply examine the mean rainfall response in the four simulations, illustrated in Fig. 14. The simulation with the HADCM3 anomaly has severely reduced rainfall over the Atlantic, as well as the Amazon, distinct from the other models used here. The explanation very likely lies in the differential warming over the tropical Atlantic and tropical Pacific, with the ratio of Atlantic to Pacific warming with HADCM3 SST clearly smaller than in any of the other models considered (see Fig. 12). The coupled simulations from the HADCM3 model in the CMIP3 database also show a distinctive severe drying over the Amazon and adjacent Atlantic Ocean. Our atmosphere-only simulations, with different atmospheric and land models, captures this distinction qualitatively, suggesting that it is primarily a result of the SST anomaly pattern and not the details of the atmosphere/land models, once the SST anomaly pattern is specified.

Fig. 15a compares the anomalies in the ASO season vertical wind shear V_s (defined as the magnitude of the vector difference between seasonal-mean winds at 850 hPa and 200 hPa) over the Atlantic main development region (MDR) [80°W - 20°W , 10°N - 25°N] in the various SST anomaly simulations with the number of hurricanes simulated by this model, including also the ensemble mean responses for each year of the 4 observed-SST simulations. The mean over the all years of these simulations is shown as well, as is the climatological-SST simulations used as a

control for the anomaly simulations. There is a clear negative correlation with coefficient of -0.8. The linear regression coefficient for the AMIP ensemble mean data points is -1.5 hurricanes/yr per m s^{-1} wind shear. This shear metric also helps explain the difference between the two climatological-SST simulations. The Reynolds SST produces fewer Atlantic storms and also stronger ASO vertical wind shear.

Fig. 15b compares the simulated Atlantic hurricane-shear relationship with observations obtained by regression of the observed hurricane count versus vertical wind shear calculated from the NCEP-NCAR reanalysis. For this comparison we use data points from all 4 individual realizations. The model produces a slope of -1.32 hurricanes/yr per m s^{-1} , similar to the observed values of -1.25 hurricanes/yr per m s^{-1} . However, the model ASO mean shear over the MDR is about 2 m s^{-1} weaker than that in NCEP-NCAR reanalysis ($\sim 10 \text{ m s}^{-1}$). The model simulated year to year variation of ASO wind shear also correlates well with the NCEP-NCAR reanalysis with a coefficient of 0.61 (not shown). This number is smaller than the model-observation correlation in hurricane count (0.83), indicating other factors may contribute to the accuracy of the simulation of interannual variation of Atlantic hurricane count besides this shear.

The fact that the shear in the main development region is a good predictor of the model hurricane counts does not necessarily imply that the dynamical influence of the shear in inhibiting storms is dominant. For example, shears can be large in this region if oceanic convection moves equator-ward, so that the mean distance from the convective center to the main development region increases and local Hadley circulations spin up baroclinic shears in the development region. In this picture, increased shear can in part be a marker for the distance to the most favorable regions for convection. It is plausible to assume that the dynamics underlying this correlation is a mix of these kinds of effects plus the direct suppression of genesis by shear.

Using all of our simulations, Fig. 16 compares the anomalies in the difference ($T_A - T_G$) between the ASO seasonal mean SST in the Atlantic MDR region (T_A) and the entire tropical ocean (T_G) with the number of hurricanes simulated by this model. Similar to Fig. 15a, the ensemble mean responses for each year of the 4 observed-SST simulations as well as the two

control climatological-SST simulations are also shown in Fig. 16. There is a clear positive correlation with coefficient greater than 0.8. The linear regression coefficient for all the data points gives 7.8 hurricanes/year per degree change in $T_A - T_G$. This $T_A - T_G$ metric explains most of the interannual variability as well as the intermodel spread in global warming projections. For the climate change experiments, in which T_G is subject to substantial warming ($\sim 2^\circ\text{C}$), it is clearly important to distinguish between the relative change of tropical Atlantic SST with respect to tropical mean from its absolute change (change of T_A only). Fig. 16 shows that for both set of experiments, only those models that project relative warming/cooling of the tropical Atlantic with respect to their tropical mean show increases/decreases of Atlantic hurricane activity despite the fact that all models project substantial local tropical Atlantic warming. Therefore, these simulations support the view that it is the change of $T_A - T_G$ that is the relevant metric to determine the sign of Atlantic hurricane frequency response to recent climate variations as well as to global warming, as discussed by Knutson et al. (2008), Swanson (2008) and Vecchi et al. (2008).

Fig. 16 shows that the $T_A - T_G$ metric also explains the difference between the two climatological-SST simulations. The difference in $T_A - T_G$ between the HadISST and the Reynolds climatological-SST is roughly 0.15° . Based on the linear fit, this gives $7.8 \times 0.15 \approx 1.2$ hurricane/year increase, which is consistent with the simulated difference (~ 1.5 hurricane/year) between the two climatological-SST simulations. This level of sensitivity is also consistent with a recent observational study by Saunders and Lea (2008).

The hurricane frequency response to 21st century SST projections is shown for other basins in Fig. 17. The atmospheric model shows an increase in frequency over the East Pacific from three of the four projections, including from the ensemble mean SST anomalies. In three of the projections, the SSTs that generate a decrease in the Atlantic show an increase in the East Pacific, and vice versa, consistent with the negative correlation on ENSO time scales (an exception is the ECHAM5 SST anomalies for which the model suggests an increase in both the Atlantic and East Pacific). In the West Pacific, the ensemble mean SST anomalies show a decrease in activity, as

does the ECHAM5 SSTs, with the other two SST's generating relatively small changes. For the North Indian Ocean, CM2.1 and ECHAM5 SST anomalies tend to produce decreased activity while HADCM3 tend to give the opposite response. The results of North Indian Ocean show much larger error bars partly due to there being fewer hurricanes over this basin. The increase of hurricane activity over the East Pacific and the North Atlantic and the decrease of activity over West Pacific and North Indian for the ECHAM5 results are consistent with [Bengtsson et al. \(2007b\)](#).

The changes in the Southern Hemisphere are more consistent across the anomaly experiments. Fig. 17g shows roughly similar magnitude ($\sim 25\%$) of decreased activities among the experiments despite some variations in the partitions of the change into different southern ocean basins (Fig. 17e-f). The relatively larger warming of the SSTs in the Northern as compared to the Southern Hemisphere tropics/subtropics, resulting in a more stable atmosphere in the south, is a plausible cause for this consistent reduction in activity.

While there is overall consistency between the two sets of climate change experiments, it appears that some of the details of the basin-wide change of hurricane frequency might also depend on the choice of the control simulation. For example, the response of South Pacific for the ENSEMBLE and CM2.1 anomalies, the response of Atlantic for the CM2.1 anomalies and the response of East Pacific for the HADCM3 anomalies show differences in magnitude when the control experiment is chosen differently.

Finally, Fig. 17h shows that seven out of the eight climate change experiments produce modest reduction of the global hurricane frequency with warming. The exception is the HADCM3 SST anomalies with the HadISST climatological-SST as the control simulation, yet this experiment does not have a change significantly different from zero. This case produces 160% increase of the East Pacific hurricane frequency, which dominates the change of both North Hemisphere and global hurricane frequency. The ensemble mean SST anomalies produce roughly 15% global reduction, of which nearly 2/3 comes from the Southern Hemisphere.

While we have relatively little confidence in the model's intensity response to global

warming, we describe it briefly here for comparison with other models from previous studies. Fig. 18a shows the change (warming minus control) in the annual count of storms with surface maximum wind speed exceeding a given value for the entire global tropical ocean. For each SST anomaly forcing, the change in storm count is averaged over the two background climatology cases. There is a global reduction of the number of tropical storms for all cases with the HADCM3 SST anomalies producing ~ 12 ($\sim 11\%$) fewer storms while the other three SST anomalies generating ~ 22 ($\sim 20\%$) fewer storms. The magnitude of the reductions decrease gradually when one moves to stronger storms. For example, for the hurricane-strength (wind-speed $> 33 \text{ m s}^{-1}$) storms, CM21, ECHAM5 and the ensemble SST anomalies produce a range of 4-8 fewer count ($\sim 8\%$ - 15%) while HADCM3 SST anomalies give a slight increase, consistent with that shown in Fig. 17h. For further stronger storms with wind-speed above 50 m s^{-1} , Fig. 18a shows an increase (instead of decrease) of storm count for all cases with CM2.1 SST anomalies generating ~ 4 ($\sim 100\%$) more storms and the other three giving a range of 0.5-1 (13-25%) increase. The annual 1 (25%) count increase of storms with intensity exceeding 50 m s^{-1} for the ECHAM5 SST anomalies is close to the value (1.2, $\sim 30\%$) obtained by Bengtsson et al. (2007b) who used a different model but similar horizontal resolution.

Fig. 18b shows the change in probability of exceedance of a given surface maximum wind (i.e., the total number of storms for each case is normalized to 1 before subtraction). A positive value indicates an increase in the fraction of storms with maximum surface wind speed above the corresponding value. The shifting towards stronger storms in warmer climate is clear for all SST anomalies with a range of 4-8% increase in the fraction of hurricane-strength storms. These numbers are roughly consistent with the fractional change (3-7%) of the mean and median wind-speed for all tropical storms between the global warming cases and the controls. The results are also comparable to the estimate ($\sim 6\%$ increase in maximum surface wind speed for a doubling of CO₂) by Knutson and Tuleya (2004). It is interesting that the ensemble SST anomalies produce the smallest intensification compared to other cases. The simulated intensity changes for individual ocean basins are broadly similar to that from the global tropical ocean shown in Fig. 18

with the largest intensification taking place in the Eastern Pacific (not shown). This result is also consistent with Bengtsson et al. (2007b). However, the quantitative estimates of intensity change with respect to global warming must be viewed with caution since storm intensities are generally not adequately resolved at this coarse resolution (see Fig 6) and any quantitative estimates of intensity response to climate change based on current global models are likely to be resolution dependent, as also pointed out by Bengtsson et al. (2007b).

5. Discussion and Conclusions

It is not a priori self-evident what horizontal resolution is needed in a global model to realistically simulate the statistics of tropical storms. Our work with a global atmospheric model, with a 50km grid spacing, adds to a growing set of encouraging results with resolution in the 20-100 km range in simulating the climatology and interannual variability of tropical storm and hurricane frequencies. The implication is that one can simulate realistic storm frequencies without simultaneously simulating a realistic distribution of storm intensities.

The model that we use here parameterizes shallow convection and allows this convection to extend as deeply as it can into the troposphere, but the large entrainment rate specified makes this difficult and forces the resolved scales to contribute much of the deep convection and precipitation in the tropics. This type of closure likely improves as the resolution becomes finer, the question being whether the distortions that result from forcing the large-scale to play a significant role at this 50 km resolution are acceptable. The diurnal cycle of precipitation is not adequately simulated in many regions, for example. We believe that the tropical storm climatology described here, as well as the quality of the large scale flow, is evidence for the value of this approach.

Averaging over four realizations of the period 1981-2005, using observed SSTs as the lower boundary condition, we find that the models year-to-year variations in Atlantic hurricane frequency are correlated with observations with a coefficient of 0.83. The implication of such high correlation is that the noise level in this statistic, that part of the Atlantic variability not explainable by variations in SST, is rather small (< 2 hurricanes/yr). This level of skill also leaves

little room for other factors not transmitted through the SST distribution, such as the stratospheric quasi-biennial oscillation or *in situ* atmospheric effects of dust variations that are not themselves forced through SSTs. The model's interannual variability in hurricane frequency is less well correlated with observations in the East, West and South Pacific, with values of roughly 0.6, 0.5, 0.3, and there is no significant correlation with the IBTrACS observed records in the Indian Ocean.

The model simulates an upward trend of hurricane frequency in the North Atlantic and a downward trend in the East and West Pacific over the 1981-2005 period. Both are consistent with the observations, with the observed trends lying within the ensemble spread of model trends. Without normalization, for the Northern Hemisphere altogether, the model produces a downward trend of -0.06 hurricane/yr close to the observed value of -0.05 hurricanes/yr. In the Southern Hemisphere, the model generates a downward trend of hurricane frequency with magnitude (-0.13 hurricanes/yr) larger than the observed value (-0.01 hurricanes/yr) from the IBTrACS dataset, although a similar magnitude downward trend does exist in observations if one takes into account all the tropical storms in the Southern Hemisphere. Globally averaged, the model ensemble mean generates a downward trend of hurricane frequency (-0.19 hurricane/yr) that is about 3 times larger than the value (-0.06 hurricane/yr) in IBTrACS.

When we perturb the SSTs with anomalies generated by global model projections for late in the 21st century, using an ensemble mean over the CMIP3 A1B simulations from 18 models, there is a reduction in the globally averaged hurricane frequency, made up from reductions in the Atlantic, the West Pacific and the Southern Hemisphere, with a substantial ($\sim 40\%$) increase in activity in the East Pacific. Despite the large differences in the specific regional changes, the global mean reduction ($\sim 15\%$) appears to be close to the value one would estimate by extrapolating the reduction simulated by the model for the period 1981-2005 ($\sim 8\%$), assuming that it is due to the tropical mean warming of SSTs. However, the fact that the ECHAM5 SST anomalies, with the largest tropical mean warming, do not produce the largest reduction also indicates an important effect of the regional SST pattern change on global hurricane frequency.

When the SST anomalies are taken from individual realizations from individual global models the results are quite varied. Globally, there is still a small ($\sim 10\%$) reduction or little change (i.e., HADCM3), but this generally is a result of larger changes in individual basins. Some of the largest basin-wide changes are projected using the SSTs from HADCM3, which generates a large increase (\sim doubling) in the East Pacific with a sharp reduction (\sim halving) in the Atlantic. The SSTs projected by CM2.1 generate the opposite pattern in the Atlantic and East Pacific, while the ECHAM5 SSTs produce modest increases in both basins. The results using individual model SSTs need to be evaluated with care, since they use individual realizations, so the spread of these results includes the sampling of low-frequency variability as well as spread in the forced responses in the different models.

Reduced activity in the Southern Hemisphere is one of the more robust responses across the models, reflecting, we presume, the robustness of the relatively small warming projected for the Southern Hemisphere tropics and subtropics as compared to that projected for the Northern tropics.

In the Atlantic, the changes in hurricane frequency are strongly correlated with the differential warming of SSTs in the Atlantic Main Development Region (T_A) with respect to the average SST of the entire tropical oceans (T_G). As discussed by [Vecchi et al. \(2008\)](#), one can build linear regression models using either T_A or $T_A - T_G$ as an explanatory variable and recover a significant representation of the model hurricane activity over the 1981-2005 period. However, the linear regression model built using T_A as a predictor is inadequate for predicting this model's response to projected 21st century SST anomaly, while that built using $T_A - T_G$ recovers much of the GCM's sensitivity to the various climate SST forcing. A multiple linear regression model for hurricane counts using T_A and T_G as separate predictors gives a best fit prediction proportional to $T_A - 1.1T_G$, which - although not significantly distinguishable from using $T_A - T_G$ as a predictor - captures a tendency for tropical-mean warming to damp hurricane activity in the Atlantic.

Physically, the differential warming can affect hurricane frequencies in several ways. It

affects the gravitational stability over the Atlantic, since the free tropospheric temperatures tend to follow the tropical mean SSTs (e.g., [Sobel et al. 2002](#)). The damping effect of tropical-mean SST on storm potential intensity ([Emanuel 1988](#)) has been shown by [Vecchi and Soden \(2007a\)](#) who demonstrated that changes in local SST are inadequate for characterizing the changes in potential intensity in greenhouse-gas warmed climates. This change of tropospheric stability presumably also impact storm genesis and frequency.

The differential warming also affects the vertical shear in the Atlantic MDR (e.g., [Latif et al. 2007](#)). As shown in both the models and the observations (Fig. 15), changes in hurricane frequency are closely related to the changes of vertical shear in the MDR. Since the changes in wind shear and atmospheric stability are likely to be strongly correlated, it is difficult to distinguish between these two mechanisms in a study of this kind, and we cannot rule out the possibility that the shear is in part a proxy for this differential stabilization or for the related north-south displacements of the ITCZ. Further, there is also evidence that some of the increased Atlantic wind shear in the global warming experiments is connected to the weakening of the Pacific Walker circulation ([Vecchi and Soden 2007b](#)) which arises from global energy and mass constraints from uniform warming ([Held and Soden 2006](#)). For sorting out the dynamical mechanisms underlying these frequency changes, regional models such as that used in [Garner et al. \(2009\)](#) may provide a flexible framework in which shear and stability can be manipulated individually.

Acknowledgments This research used resources of the National Energy Research Scientific Computing Center, which is supported by the Office of Science of the U.S. Department of Energy under Contract No. DE-AC02-05CH11231. The authors thank C. Bretherton for making available the original University of Washington shallow convection scheme, S. Klein for making available the simplified stratiform cloud scheme, C. Golaz for the improvement in the iteration method in the shallow convection scheme, J. Sirutis for consultant on storm tracking algorithm, C. Kerr and V. Balaji for facilitating the computations on the DOE computers. We also thank T. Knutson and S. Garner for valuable discussions on the interpretation of these results. We acknowledge the

various IPCC modelling groups for providing their data, and PCMDI and the IPCC Data Archive at LLNL/DOE for collecting, archiving and making the data readily available. Ming Zhao was supported in part by NSF Grant ATM-0612551 and in part under award NA17RJ2612 from the National Oceanic and Atmospheric Administration, U.S. Department of Commerce. The findings are those of the authors and do not necessarily reflect the views of the National Oceanic and Atmospheric Administration, or the U.S. Department of Commerce.

6. Appendix

a. Convective and stratiform cloud parameterization

The convection scheme is adapted from the shallow cumulus scheme originally developed by [Bretherton et al. \(2004\)](#). Our primary modifications to the scheme are as follows. Liquid/frozen water static energy is used instead of liquid-frozen water potential temperature as a conserved variable. Only saturated mixtures are detrained into the large-scale stratiform clouds, for consistency with the underlying mixing assumption. A simple treatment of precipitation microphysics is included within the convection module, assuming a symmetric triangle distribution of total condensate with a width of 0.5 g kg^{-1} and with condensate above a threshold value q_{c0} removed as precipitation (the default value of q_{c0} is 1 g kg^{-1}). The iterative method for obtaining temperature from the conserved variables is refined to better handle mixed phase cloud. The boundary layer turbulent kinetic energy which enters the mass flux closure, is estimated diagnostically based on surface stress and buoyancy flux following [Holtslag and Boville \(1993\)](#), since this model has no prognostic turbulent kinetic energy equation. The upper limit in the vertical extent of the convective clouds is removed. Finally, as described in the text, the empirical non-dimensional parameter controlling the strength of the lateral mixing [c_0 in Eq. 18 in [Bretherton et al. \(2004\)](#)] is modified so that it is c_o over ocean and αc_o over land. α is a resolution dependent tunable parameter. For c48, c90 and c180 models, we set α is 0.5, 0.65, and 0.85 respectively. The value of c_0 over the ocean is 10.

The stratiform cloud scheme in AM2 ([Anderson et al. 2004](#)) is modified by removing the [Tiedtke \(1993\)](#) prognostic cloud fraction scheme and replacing it with a simpler diagnostic scheme assuming a sub-grid scale distribution of total water, provided to us by S. Klein. The distribution of total water has the form of beta distribution with the lower and upper bounds determined by a width parameter multiplied by the grid-box mean total water. For this study, both shape parameter p and q (see Eq. 7 in [Tompkins 2002](#)) are set to be 5 resulting in a symmetric distribution and the width parameter is set to 0.2. The use of the diagnostic scheme for condensation/evaporation

processes allows one to remove AM2 [Tiedtke \(1993\)](#) cloud condensation, dissipation and erosion parameterizations while still keep the general form of the prognostic condensate equations. The remainder of the stratiform cloud scheme, including its treatment of cloud microphysics and precipitation fallout, is unmodified from AM2.1.

b. Tropical cyclone detection and tracking algorithm

b.1. Algorithm The tropical cyclone detection and tracking algorithm is a 3-step procedure adapted from earlier work by [Knutson et al. \(2007\)](#) and [Vitart et al. \(1997 2003\)](#) with some simplifications/modifications for this study.

Step 1: potential storm identification. Using 6-hourly data, grid points in space and time satisfying the following conditions are located:

- At each time, 850 hPa relative vorticity maximum exceeding $1.6 \times 10^{-4} \text{ s}^{-1}$ are located within areas of $6^\circ \times 6^\circ$ latitude and longitude .
- The local minimum of sea level pressure, which must be within a distance of 2° latitude or longitude from the vorticity maximum, is defined as the center of the storm. And the local maximum surface (lowest model level) wind speed is recorded.
- The local maximum temperature averaged between 300 and 500 hPa is defined as the center of the warm core. The distance of the warm-core center from the storm center must not exceed 2° . The warm-core temperature must be at least 1° C warmer than the surrounding local mean.

Differing from [Knutson et al. \(2007\)](#), this algorithm does not use a bicubic spline method for locating maxima, minima and computing gradients, due to the large computational cost as well as the fact that little impact has been found when using this refinement with this 50km resolution data.

Step 2: storm tracking. After a database of potential storm snapshots satisfying the above conditions is created, a trajectory analysis is performed to link these together using the following

procedure:

- For each storm snapshot, a check is performed to see if there are storms during the following 6-hour time period within a distance of 400 km.
- If there are none, the trajectory is considered to have stopped. If there are some, the closest storm is chosen as belonging to the same trajectory as the initial storm. If there is more than one possibility, preference is given to storms that are to the west and poleward of the current location.
- To qualify as the model storm trajectory, a trajectory must last at least 3 days, and have a maximum surface wind speed greater than 17 ms^{-1} during at least 3 days (not necessarily consecutive).

Step 3: storm categorization. A tropical storm is categorized as a hurricane if the maximum surface wind speed at some point during its entire trajectory exceeds 33 ms^{-1} .

b.2. Sensitivity and justification for parameter choices The surface wind output from the model is the instantaneous wind field at a model time-step (15-min) from the lowest model level ($\sim 35\text{m}$). The wind is not spatially or temporally averaged and the output frequency is six hourly. When comparing with the observed storm wind, the overestimates (10-20%) due to slightly higher sampling level (35m vs. 10m) are roughly compensated by the underestimates as a result of the model's coarser spatial (50km vs. 1km) and time (15-min vs. 1-min) resolution (e.g., [Kruk et al. 2008](#)). This choice is consistent with a recent study on the resolution dependence of tropical cyclone detection algorithms for climate models ([Walsh et al. 2007](#)).

We have found some sensitivity of the resulting storm climatology to the choice of the parameters (e.g., storm duration criteria, warm-core and vorticity threshold) used in the storm detection and tracking algorithm. In particular, we find fairly large sensitivity of storm count to the threshold criteria required for storm duration. For example, the North Atlantic storm count decreases by roughly 20% when we change the storm duration criterion from 2 days to

3 days. However, when considering hurricane strength storms (with surface maximum wind speed exceeding 33 m s^{-1} in the vicinity of the storm), the reduction is less than 5%. From the IBTrACS observations we find very few hurricane strength storms have durations less than 3 days. For example, for the period of 1981-2005, globally less than 1% of hurricanes each year having durations less than 3 days while roughly 11% of tropical storms have durations less than 3 days. Furthermore, we find the sensitivity of storm count to other parameters such as the thresholds for warm-core and vorticity is also greatly reduced when we focus on stronger storms, consistent with the results of [Walsh et al. \(2007\)](#). For example, halving our vorticity threshold doesn't change hurricane climatology at all since it is the wind speed that define hurricanes and all hurricane strength storms have vorticity larger than our specified threshold value [i.e., $1.6 \times 10^{-4} \text{ s}^{-1}$ also used in [Knutson et al. \(2007\)](#)]. However, our choice of relatively larger value, compared to those used by others in coarser resolution models [i.e., $0.1 \times 10^{-4} - 0.7 \times 10^{-4} \text{ s}^{-1}$ ([Walsh et al. 2007](#))], makes storm searching computationally more efficient.

Another interesting sensitivity is that a smaller threshold for warm-core results in longer individual tracks without significantly changing hurricane counts. The use of small warm-core threshold is also supported by the results of [Walsh et al. \(2007\)](#). Since model storm tracks are typically shorter than the observed tracks [this is especially true for the IBTrACS, which shows systematically longer tracks than those from the JTWC (Joint Typhoon Warning Center) data set], we choose a relatively small warm-core temperature threshold (1°C) to optimize our simulated storm tracks.

References

- Anderson, J., V. Balaji, A. Broccoli, W. Cooke, T. Delworth, K. Dixon, L. Donner, K. Dunne, S. Freidenreich, S. Garner, R. Gudgel, C. Gordon, I. Held, R. Hemler, L. Horowitz, S. Klein, T. Knutson, P. Kushner, A. Langenhost, N.-C. Lau, Z. Liang, S. Malyshev, M. Nath, J. Ploshay, V. Ramaswamy, M. Schwarzkopf, E. Shevliakova, J. Sirutis, B. Soden, W. Stern, L. Thompson, McLean, R. Wilson, A. Wittenberg and B. Wyman, 2004: The new GFDL global atmosphere and land model AM2/LM2: Evaluation with prescribed SST simulations. *J. Climate*, **17**, 4641–4673.
- Bender, M. A., I. Ginis and Y. Kurihara, 1993: Numerical simulations of tropical cyclone-ocean interaction with a high-resolution coupled model. *J. Geophys. Res.*, **98**, 23245–23263.
- Bengtsson, L., K. Hodges and M. Esch, 2007a: Tropical cyclones in a T159 resolution global climate model: comparison with observations and re-analyses. *Tellus*, **59A**, 396–416.
- Bengtsson, L., K. Hodges, M. Esch, N. Keenlyside, L. Kornbluh, J.-J. Luo and T. Yamagata, 2007b: How may tropical cyclones change in a warmer climate. *Tellus*, **59A**, 539–561.
- Bretherton, C. S., J. R. McCaa and H. Grenier, 2004: A new parameterization for shallow cumulus convection and its application to marine subtropical cloud-topped boundary layers. Part I: Description and 1-d results. *Mon. Wea. Rev.*, **132**, 864–882.
- Delworth, T., A. Broccoli, A. Rosati, R. Stouffer, V. Balaji, J. Beesley, W. Cooke, K. Dixon, J. Dunne, K. Dunne, J. Durachta, K. Findell, P. Ginoux, A. Gnanadesikan, C. Gordon, S. M. Briffies, R. Gudgel, M. Harrison, I. Held, R. Hemler, L. Horowitz, S. Klien, T. Knutson, P. J. Kushner, A. Langenhorst, H.-C. Lee, S.-J. Lin, J. Lu, S. Schwarzkopf, E. Shevliakova, J. Sirutis, M. Spelman, W. Stern, M. Winton, A. Wittenberg, B. Wyman, F. Zeng and R. Zhang, 2006: GFDL's CM2 global coupled climate models - Part I: Formulation and simulation characteristics. *J. Climate*, **19**, 643–674.
- Douville, H., 2005: Limitations of time-slice experiments for predicting regional climate change over South Asia. *Climate Dynamics*, **24**, 373–391.

- Emanuel, K., R. Sundararajan and J. Williams, 2008: Hurricanes and global warming: results from downscaling ipcc ar4 simulations. *Bull. Amer. Meteor. Soc.*, pp. 347–367.
- Emanuel, K. A., 1988: The maximum intensity of hurricanes. *J. Atmos. Sci.*, **45**, 1143–1155.
- Garner, S., I. Held, T. Knutson and J. Sirutis, 2009: The roles of wind shear and thermodynamic stability in past and projected changes of Atlantic tropical-cyclone activity. *J. Climate*, *submitted*.
- Gualdi, S., E. Scoccimarro and A. Navarra, 2008: Changes in tropical cyclone activity due to global warming: results from a high-resolution coupled general circulation model. *J. Climate*, **21**, 5204–5228.
- Held, I. M. and R. J. Soden, 2006: Robust responses of the hydrological cycle to global warming. *J. Climate*, **19**, 5686–5699.
- Holtslag, A. A. M. and B. A. Boville, 1993: Local versus nonlocal boundary-layer diffusion in a global climate model. *J. Climate*, **6**, 1825–1842.
- Kain, J. S. and J. M. Fritsch, 1990: A one-dimensional entraining/detraining plume model and its application in convective parameterization. *J. Atmos. Sci.*, **47**, 2784–2802.
- Kalnay, E., M. Kanamitsu and et.al, 1996: The NCEP/NCAR 40-year reanalysis project. *Bull. Amer. Meteor. Soc.*, **77**, 437–471.
- Knutson, T., J. Sirutis, S. Garner, I. Held and R. E. Tuleya, 2007: Simulation of the recent multidecadal increase of Atlantic hurricane activity using an 18-km-grid regional model. *Bull. Amer. Meteor. Soc.*, pp. 1549–1565.
- Knutson, T., J. Sirutis, S. Garner, G. Vecchi and I. Held, 2008: Simulated reduction in Atlantic hurricane frequency under twenty-first-century warming condition. *Nature Geoscience*, p. doi:10.1038/ngeo202.
- Knutson, T. K. and R. E. Tuleya, 2004: Impact of co2-induced warming on simulated hurricane

- intensity and precipitation: Sensitivity to the choice of climate model and convective parameterization. *J. Climate*, **17**, 3477–3495.
- Kruk, M., K. Knapp, D. Levinson and J. Kossin, 2008: A technique for merging global tropical cyclone best track data. *J. Atmos. Oceanic Tech.*, *submitted*.
- LaRow, T., Y.-K. Lim, D. Shin, E. Chassignet and S. Cocke, 2008: Atlantic basin seasonal hurricane simulations. *J. Climate*, **21**, 3191–3206.
- Latif, M., N. Keenlyside and J. Bader, 2007: Tropical sea surface temperature, vertical wind shear, and hurricane development. *Geophys. Res. Lett.*, **34**, L01710, doi:10.1029/2006GL027969.
- Lau, N.-C. and J. J. Ploshay, 2009: Simulation of synoptic and sub-synoptic scale phenomena associated with the East Asian summer monsoon using a high-resolution GCM. *Mon. Wea. Rev.*, *submitted*.
- Lin, S.-J., 2004: A "vertically lagrangian" finite-volume dynamical core for global models. *Mon. Wea. Rev.*, **132**, 2293–2307.
- Lin, S.-J. and R. B. Rood, 1996: Multidimensional flux-form semi-lagrangian transport schemes. *Mon. Wea. Rev.*, **124**, 2046–2070.
- Meehl, G., C. Covey, T. Delworth, M. Latif, B. McAvaney, J. Mitchell, R. Stouffer and K. Taylor, 2007: The WCRP CMIP3 multimodel dataset: A new era in climate change research. *Bull. Amer. Meteor. Soc.*, pp. 1383–1394.
- Oouchi, K., J. Yoshimura, H. Yoshimura, R. Mizuta, S. Kusunoki and A. Noda, 2006: Tropical cyclone climatology in a global-warming climate as simulated in a 20 km mesh global atmospheric model: Frequency and wind intensity analysis. *J. Meteor. Soc. Japan*, **84**, 259–276.
- Park, S. and C. S. Bretherton, 2009: The University of Washington shallow convection and moist turbulence schemes and their impact on climate simulations with the Community Atmosphere Model. *J. Climate*, *revised, 10 2008*.

- Putman, W. M. and S.-J. Lin, 2007: Finite-volume transport on various cubed-sphere grid. *J. Comput. Phys.*, **227**, 55–78.
- Rayner, R., D. Parker, E. Horton, C. Folland, L. Alexander and D. Rowel, 2003: Global analyses of sea surface temperature, sea ice, and night marine air temperature since the late nineteenth century. *J. Geophys. Res.*, **108**, D14,4407,doi:10.1029/2002JD002670.
- Reynolds, R., N. Rayner, T. Smith, D. Stokes and W. Wang, 2002: An improved in situ and satellite SST analysis for climate. *J. Climate*, **15**, 1609–1625.
- Santer, B., P. Thorne, L. Haimberger, K. Taylor, T. Wigley, J. Lanzante, S. Solomon, M. Free, P. Gleckler, P. Jones, T. Karl, S. Klein, C. Mears, D. Nychka, G. Schmidt, S. Sherwood and F. Wentz, 2008: Consistency of modelled and observed temperature trends in the tropical troposphere. *Int. J. Climatol.*, p. DOI:10.1002/joc.
- Saunders, M. and A. Lea, 2008: Large contribution of sea surface warming to recent increase in Atlantic hurricane activity. *Nature*, **451**, 557–561 doi:10.1038/nature06423.
- Schade, L. and K. Emanuel, 1999: The ocean's effect on the intensity of tropical cyclones: results from a simple coupled atmosphere-ocean model. *J. Atmos. Sci.*, **56**, 642–651.
- Sobel, A., I. Held and C. Bretherton, 2002: The ENSO signal in tropospheric temperature. *J. Climate*, **15**, 2702–2706.
- Swanson, K. L., 2008: Non-locality of Atlantic tropical cyclone intensities. *Geochem. Geophys. Geosys.*, p. doi:10.1029/2007GC001844.
- Tiedtke, M., 1993: Representation of clouds in large-scale models. *Mon. Wea. Rev.*, **121**, 3040–3061.
- Tompkins, A. M., 2002: A prognostic parameterization for the subgrid-scale variability of water vapor and clouds in large-scale models and its use to diagnose cloud cover. *J. Atmos. Sci.*, **59**, 1917–1942.

- Vecchi, G. and B. Soden, 2007a: Effect of remote sea surface temperature change on tropical cyclone potential intensity. *Nature*, **450**, 1066–1071 doi:10.1038/nature06423.
- Vecchi, G. and B. Soden, 2007b: Increased tropical Atlantic wind shear in model projections of global warming. *Geophys. Res. Lett.*, **34**, L08702, doi:10.1029/2006GL028905.
- Vecchi, G., K. Swanson and B. Soden, 2008: Whither hurricane activity. *Nature*, **322**, 687–689.
- Vitart, F., 2006: Seasonal forecasting of tropical storm frequency using a multi-model ensemble. *Q. J. R. Meteorol. Soc.*, **132**, 647–666.
- Vitart, F., D. Anderson and T. Stockdale, 2003: Seasonal forecasting of tropical cyclone landfall over Mozambique. *J. Climate*, **16**, 3932–3945.
- Vitart, F., J. Anderson and W. Stern, 1997: Simulation of interannual variability of tropical storm frequency in an ensemble of gcm integrations. *J. Climate*, **10**, 745–760.
- Vitart, F., M. Huddleston, D. Deque, D. Peake, T. Palmer, T. Stockdale, M. Davey, S. Ineson and A. Weisheimer, 2007: Dynamically-based seasonal forecasts of Atlantic tropical storm activity issued in June by EUROSIP. *Geophys. Res. Lett.*, **34**, L16815, doi:10.1029/2007GL030740.
- Waliser, D., K. Lau and J.-H. Kim, 1999: The influence of coupled sea surface temperatures on the Madden-Julian oscillation: A model perturbation experiment. *J. Atmos. Sci.*, **56**, 333–358.
- Walsh, K., M. Fiorino, C. Landsea and K. McInnes, 2007: Objectively determined resolution-dependent threshold criteria for the detection of tropical cyclones in climate models and reanalyses. *J. Climate*, **20**, 2307–2314.
- Xie, P. and P. Arkin, 1996: Global precipitation: a 17-year monthly analysis based on gauge observations, satellite estimates, and numerical model outputs. *Bull. Amer. Meteor. Soc.*, **78**, 2539–2558.

This manuscript was prepared with AGU's \LaTeX macros v4, with the extension package 'AGU++' by P. W. Daly, version 1.6b from 1999/08/19.

Figure captions list

Figure 1: Sensitivity of annual mean Amazon precipitation to horizontal resolution and cumulus lateral mixing rate over land. Left column (panel a,b,c): the same physics except for the indicated resolution change, with a fixed ratio of land to ocean lateral mixing rates of $\alpha=0.85$. Right column: panel d: as in a) except $\alpha=0.5$; panel e: as in b) except $\alpha=0.65$; panel f: observations from Climate Prediction Center Merged Analysis of Precipitation data (CMAP, [Xie and Arkin 1996](#)). Unit: mm day^{-1} .

Figure 2: A comparison of RMS error (normalized by observed standard deviation of spatial variation of each time-mean field) of selected fields from the C180, C90, C48 HIRAM2.1 and the standard AM2.1 integrations with prescribed SSTs (1981-2005). The boxes show the lower quartiles, medians (red lines), and upper quartiles of 10 other model runs from the CMIP3 data base, while the whiskers show the max and min values among these models. a) Precipitation compared to CMAP; b) Northern Hemisphere sea level pressure (compared to NCEP-NCAR reanalysis); c) 850 hPa zonal wind (compared to NCEP-NCAR reanalysis); d) As in c) but for 200 hPa zonal wind.

Figure 3: A comparison of observed (upper panel) and model simulated (lower panel) hurricane tracks from 1981 to 2005.

Figure 4: A comparison of observed and simulated annual mean hurricane count for each ocean basin averaged over 1981 to 2005. M1, M2, M3, M4 represent each integration of the 4-member ensemble.

Figure 5: Observed and model simulated seasonal cycle (number of hurricanes per month) for each ocean basin from the 4-member ensemble mean (1=JAN, 12=DEC).

Figure 6: A comparison of observed and model simulated tropical storm intensity distribution as characterized by the surface maximum wind speed for North Atlantic (upper), East Pacific (middle) and West Pacific (bottom). Black: IBTrACS observations using 1-min maximum sustained wind at 10m. Red: model simulation using 15-min (model time-step) winds at the

lowest model level.

Figure 7: Interannual variation of hurricane numbers for North Atlantic from 1981 to 2005. Red: IBTrACS observations (Kruk et al. 2008); blue: 4-member ensemble mean; shaded area shows the simulated maximum and minimum number for each year from the 4 member integrations. Model time series are normalized by time-independent multiplicative factors so as to reproduce the observed total number. Dotted lines show observed and model (ensemble mean) linear trends.

Figure 8: A comparison of observed and model simulated hurricane tracks for year 2005. Upper panel: observed tracks; middle and bottom panels: simulated tracks from each individual realization of the 4-member ensemble. Yellow dots show the locations where maximum wind speed exceeds 33 m s^{-1} along each track.

Figure 9: As in Fig. 7 except for the East Pacific.

Figure 10: As in Fig. 7 except for the West Pacific.

Figure 11: Upper panel: the correlation of observed hurricane count to the 4-member ensemble mean (stars) and the correlation of each ensemble member to the ensemble mean of the remaining three (circles) for each basin. Lower panel: observed (stars) and modeled (circles) linear trends in hurricane frequency for the period 1981-2005 in each basin. Model trends are from individual realizations and calculated from normalized time series.

Figure 12: Aug-Sept-Oct seasonal mean SST anomaly from a) GFDL CM2.1, b) UKMO HADCM3, c) MPI ECHAM5 and d) multi-model ensemble mean (see detailed description in the text). Unit: $^{\circ} \text{K}$.

Figure 13: Fractional changes in annual hurricane (left) and tropical storm (right) count for the North Atlantic basin from the 4 SST anomaly simulations based on 2 different control climatological-SSTs. Error bars show the 90% confidence level assuming the sampling distributions are normally distributed. Legend shows the two control climatological-SSTs.

Figure 14: Aug-Sept-Oct seasonal mean precipitation differences between SST anomaly simulations and the control simulation. Unit: mm day^{-1} .

Figure 15: a) Scatter plot of annual Atlantic hurricane count versus ASO season vertical wind

shear anomalies from the ensemble mean for each year of the 4 observed-SST simulations (small pentagrams). The big pentagram shows the AMIP all-year mean and the line is a linear regression of the 25 year data points. Also shown are results from the two control climatological-SST simulations (red symbols) and the various SST anomaly simulations (green: ENSEMBLE, blue: CM2.1, black: HADCM3, cyan: ECHAM5). Squares denote the set of experiments using Reynolds climatological-SST as a control, circles denote the set of experiments using HadISST climatological-SST as a control. For the control and SST anomaly simulations, the ASO wind shear anomalies are the mean ASO wind shear minus the AMIP all-year mean. b) As in a) except showing all members of the AMIP runs with all climate change experiments removed. Black circles show scatter plots of observed Atlantic hurricane count versus vertical wind shear calculated from NCEP-NCAR reanalysis. The red and black lines are respectively linear regression of the model and observation data points.

Figure 16: As in Fig. 15a except for scatter plot of annual Atlantic hurricane count versus ASO season Atlantic MDR SST (T_A) minus tropical mean SST (T_G); $T_A - T_G$ is shown as anomalies from the climatological value obtained for the period of 1981-2005.

Figure 17: Fractional changes in annual hurricane counts (as in Fig 13a) except for a) East Pacific, b) West Pacific c) North Indian, d) Northern Hemisphere, e) South Pacific, f) South Indian, g) Southern Hemisphere, and h) the global ocean. Error bars show the 90% confidence level assuming the sampling distributions are normally distributed.

Figure 18: a) Change (warming minus control) in annual storm count exceeding a given surface maximum wind for the entire global tropical ocean. Vertical lines show the lower quartile, median, and upper quartile of the controls. b) As in a) but show change in the probability of exceedance of tropical storm intensity. Positive value indicates relative increase in the fraction of storms with maximum surface wind speed above the corresponding value.

Figure Captions

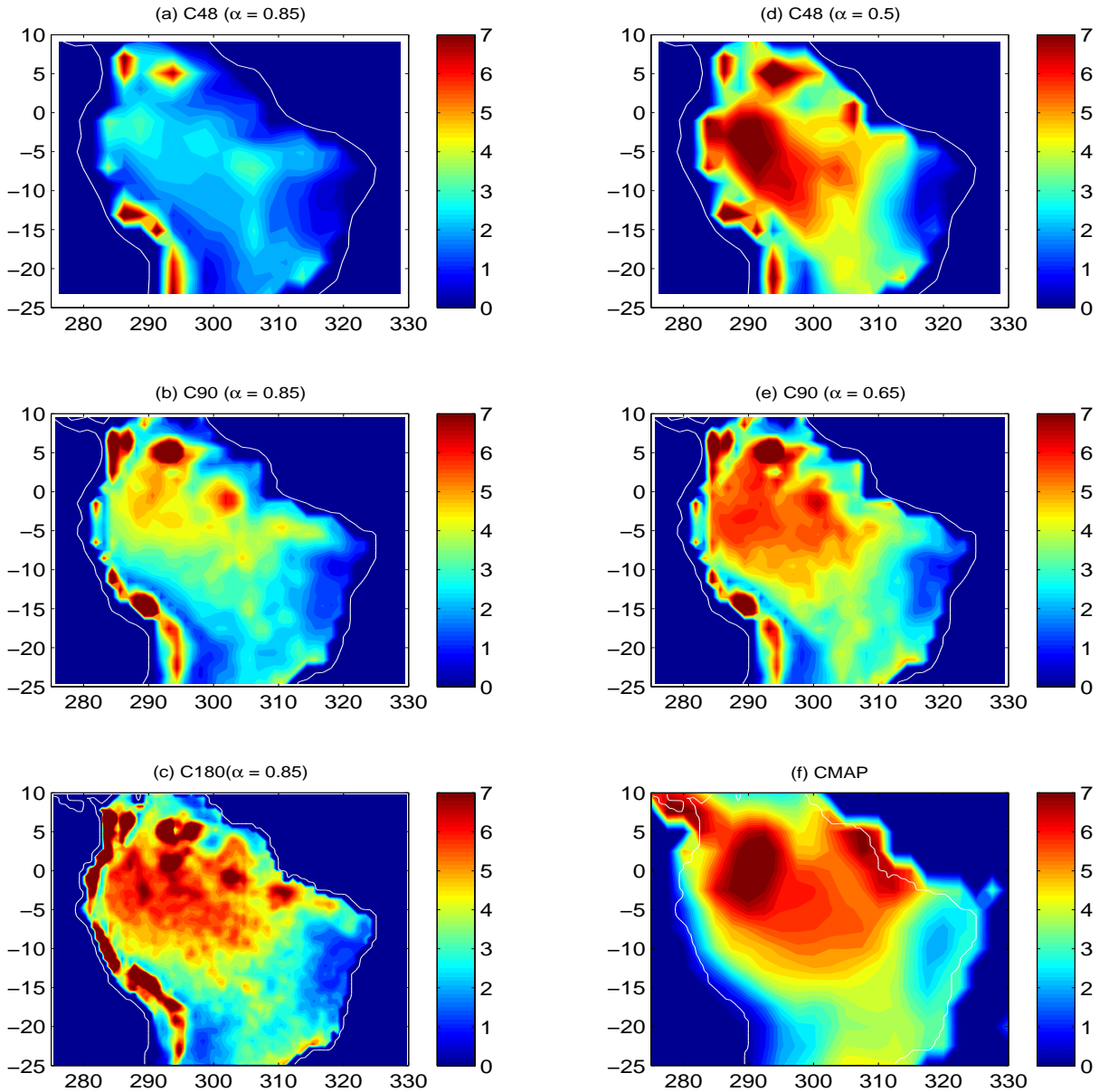


Figure 1. Sensitivity of annual mean Amazon precipitation to horizontal resolution and cumulus lateral mixing rate over land. Left column (panel a,b,c): the same physics except for the indicated resolution change, with a fixed ratio of land to ocean lateral mixing rates of $\alpha=0.85$. Right column: panel d: as in a) except $\alpha=0.5$; panel e: as in b) except $\alpha=0.65$; panel f: observations from Climate Prediction Center Merged Analysis of Precipitation data (CMAP, Xie and Arkin 1996). Unit: mm day⁻¹.

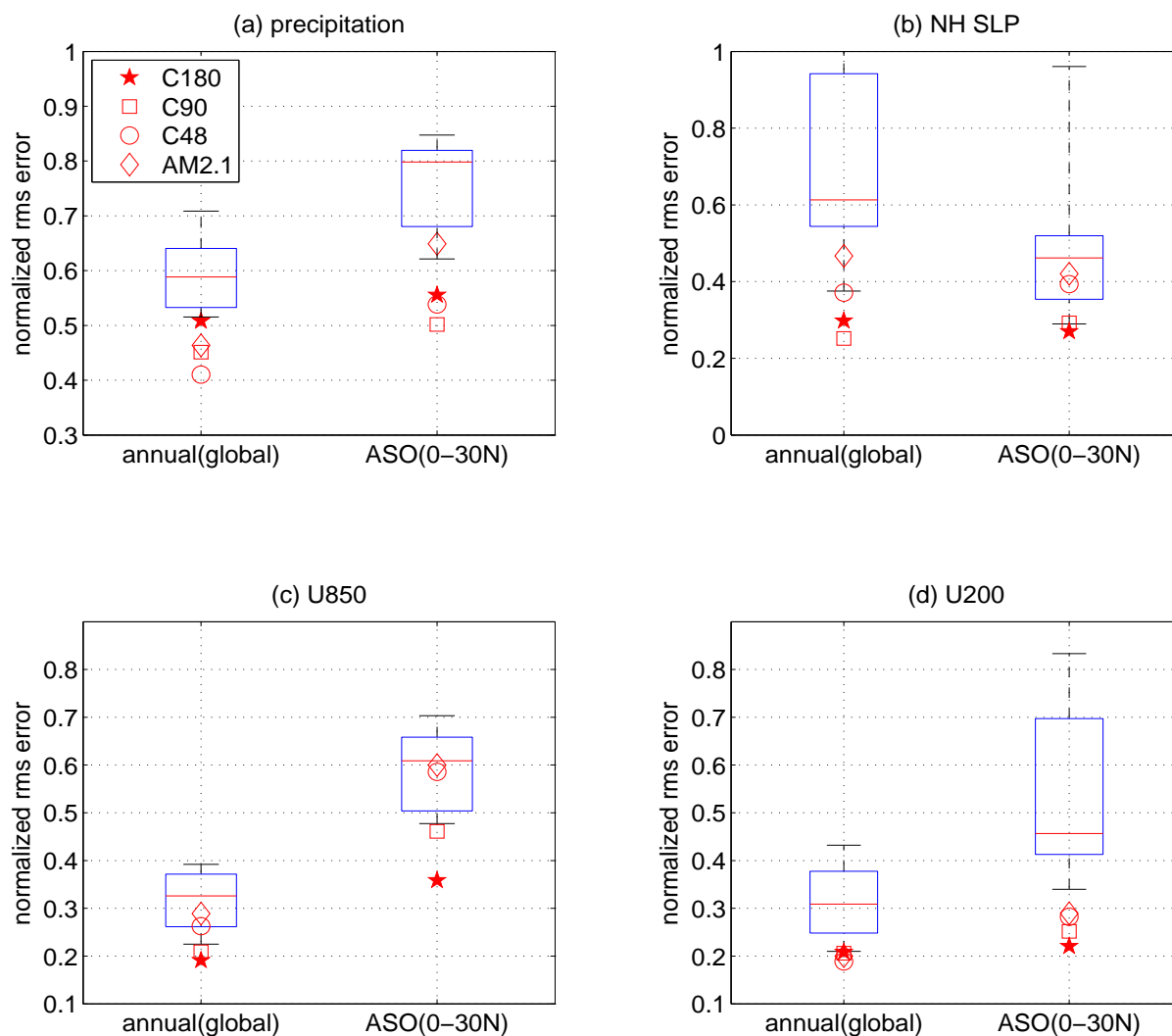


Figure 2. A comparison of RMS error (normalized by observed standard deviation of spatial variation of each time-mean field) of selected fields from the C180, C90, C48 HIRAM2.1 and the standard AM2.1 integrations with prescribed SSTs (1981-2005). The boxes show the lower quartiles, medians (red lines), and upper quartiles of 10 other model runs from the CMIP3 data base, while the whiskers show the max and min values among these models. a) Precipitation compared to CMAP; b) Northern Hemisphere sea level pressure (compared to NCEP-NCAR reanalysis); c) 850 hPa zonal wind (compared to NCEP-NCAR reanalysis); d) As in c) but for 200 hPa zonal wind.

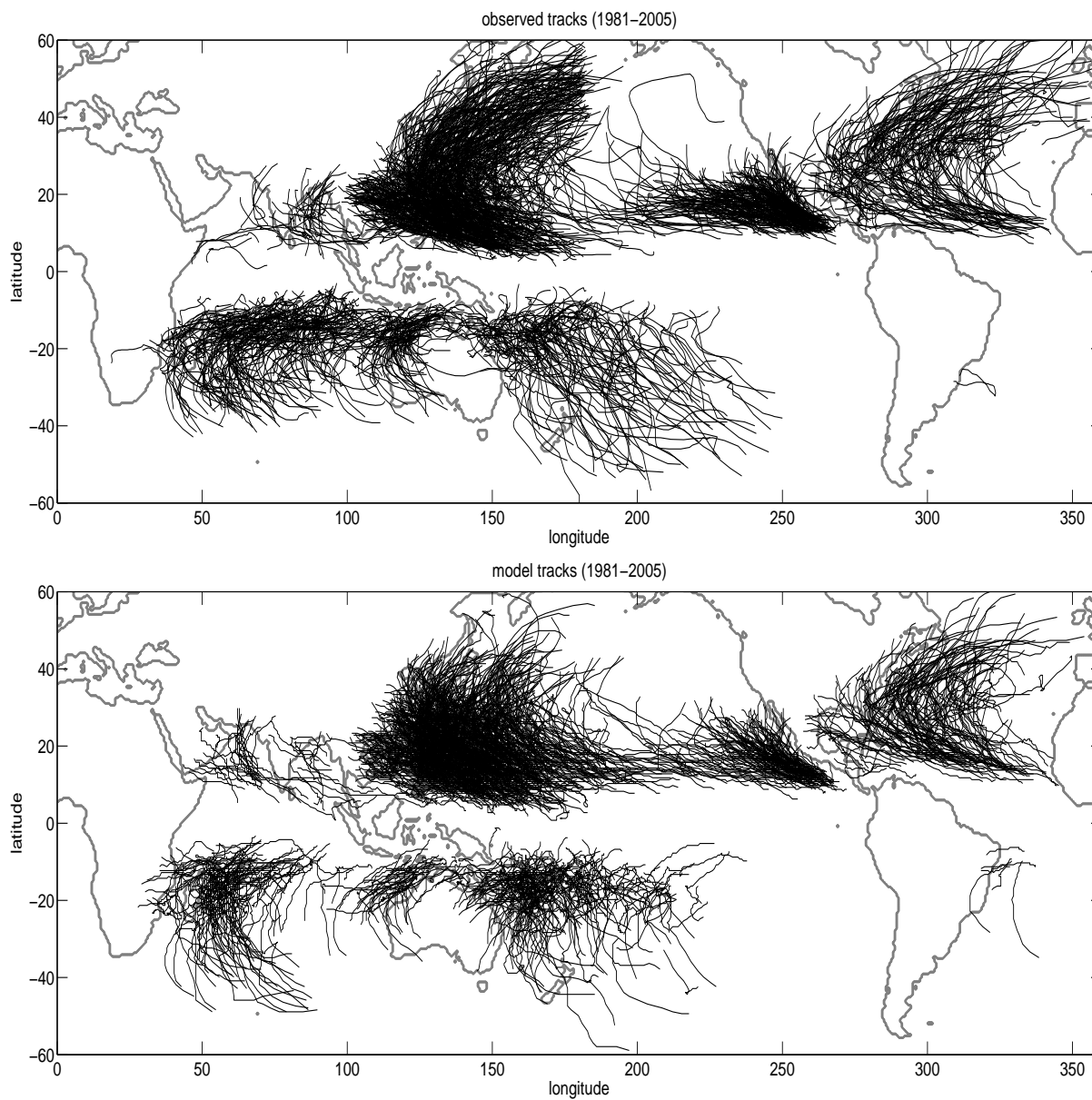


Figure 3. A comparison of observed (upper panel) and model simulated (lower panel) hurricane tracks from 1981 to 2005.

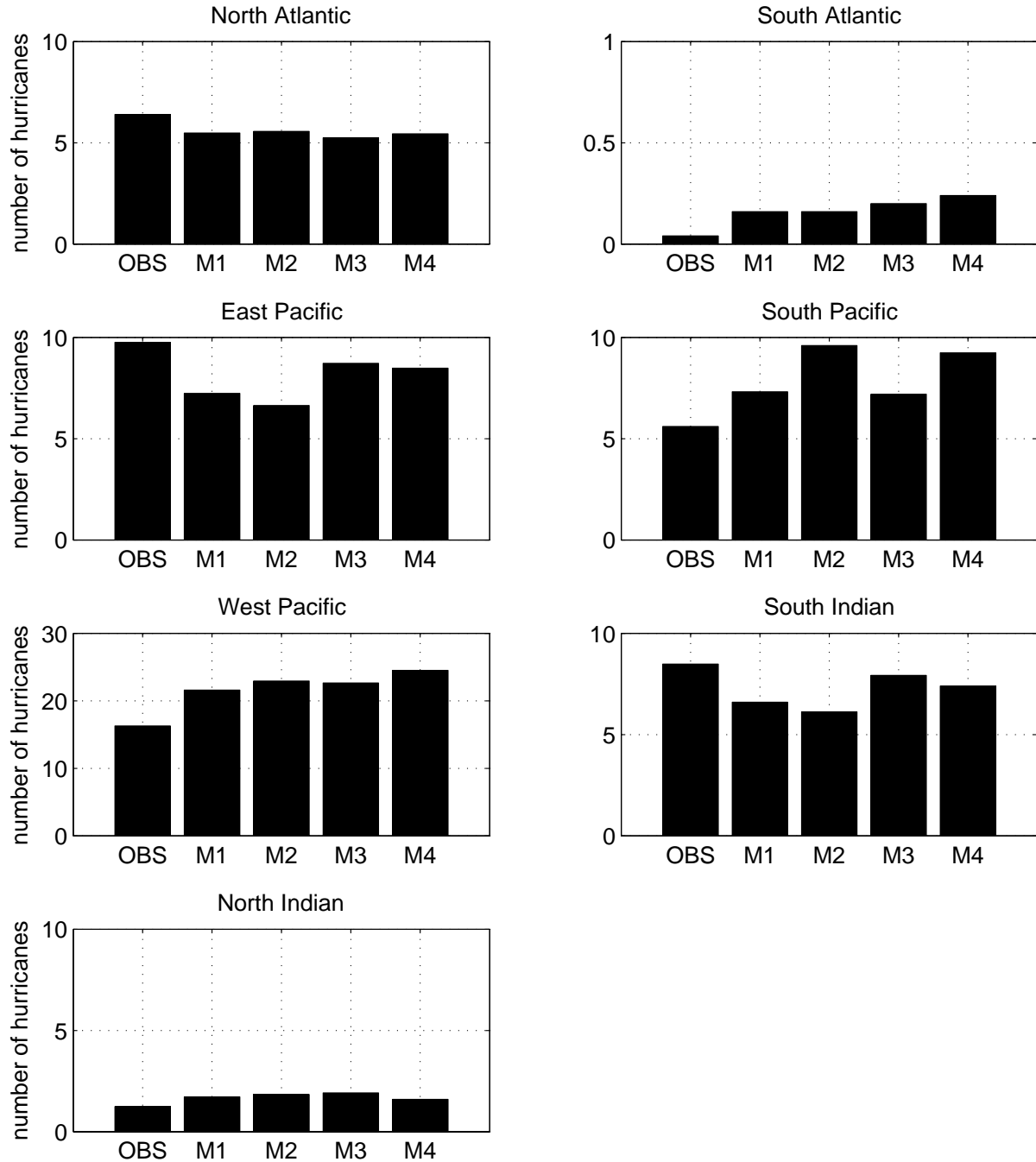


Figure 4. A comparison of observed and simulated annual mean hurricane count for each ocean basin averaged over 1981 to 2005. M1, M2, M3, M4 represent each integration of the 4-member ensemble.

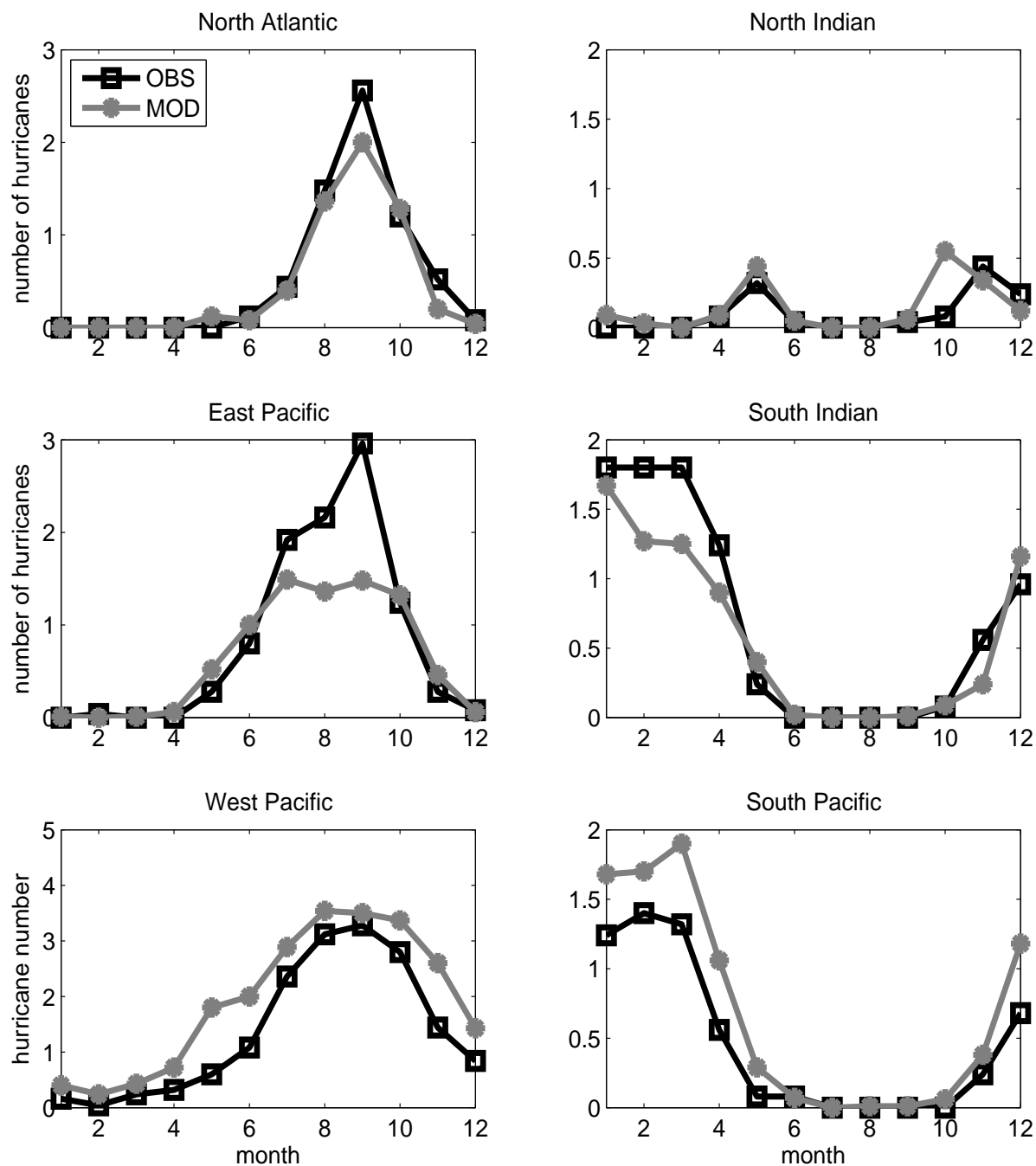


Figure 5. Observed and model simulated seasonal cycle (number of hurricanes per month) for each ocean basin from the 4-member ensemble mean (1=JAN, 12=DEC).

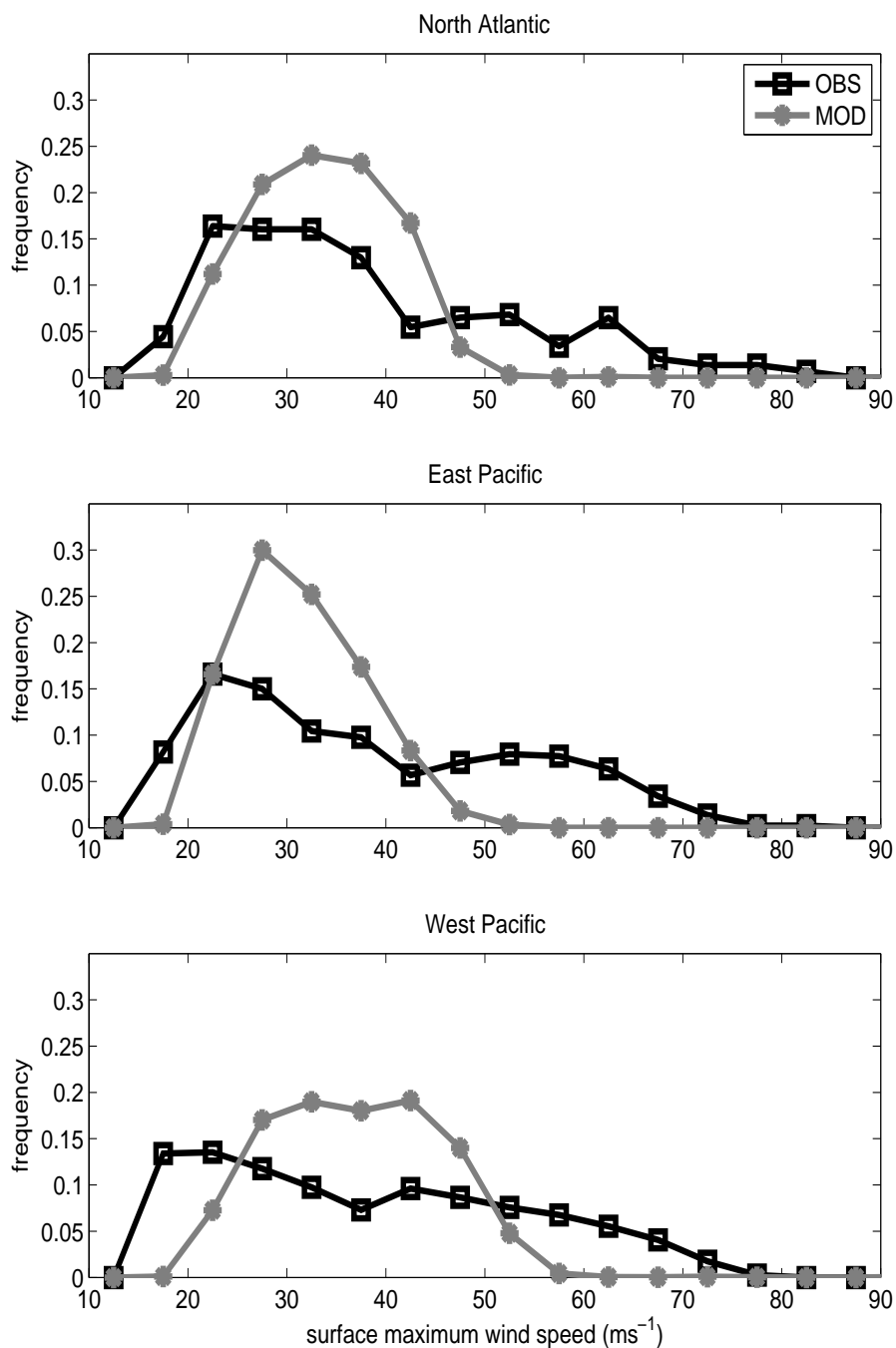


Figure 6. A comparison of observed and model simulated tropical storm intensity distribution as characterized by the surface maximum wind speed for North Atlantic (upper), East Pacific (middle) and West Pacific (bottom). Black: IBTrACS observations using 1-min maximum sustained wind at 10m. Red: model simulation using 15-min (model time-step) winds at the lowest model level.

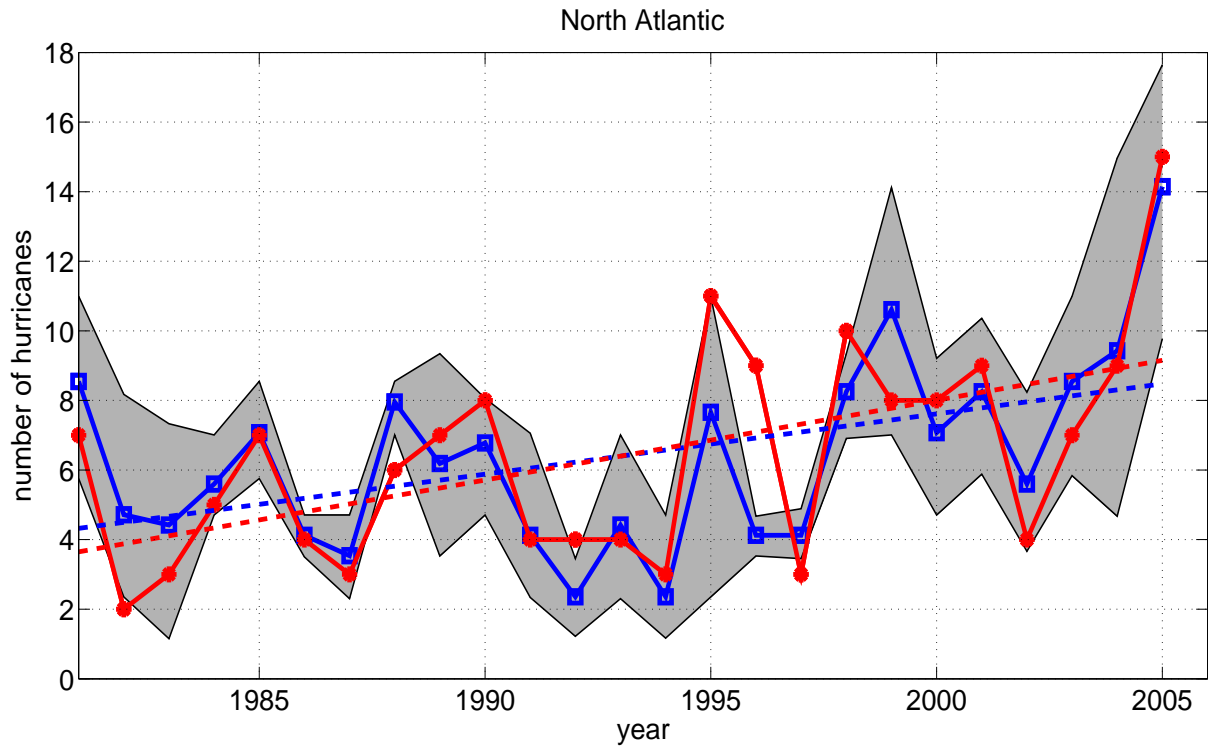


Figure 7. Interannual variation of hurricane numbers for North Atlantic from 1981 to 2005. Red: IBTrACS observations (Kruk et al. 2008); blue: 4-member ensemble mean; shaded area shows the simulated maximum and minimum number for each year from the 4 member integrations. Model time series are normalized by time-independent multiplicative factors so as to reproduce the observed total number. Dotted lines show observed and model (ensemble mean) linear trends.

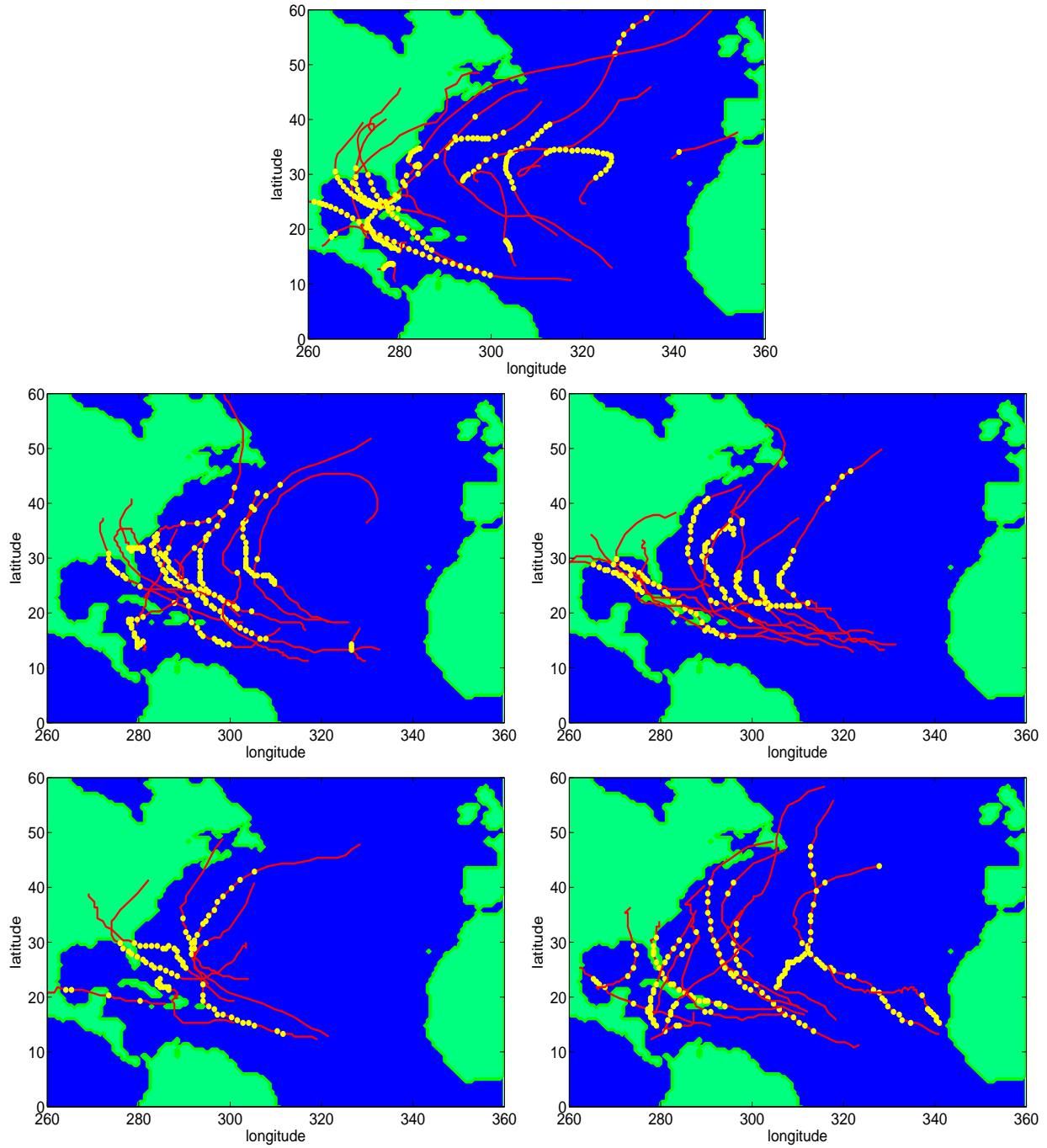


Figure 8. A comparison of observed and model simulated hurricane tracks for year 2005. Upper panel: observed tracks; middle and bottom panels: simulated tracks from each individual realization of the 4-member ensemble. Yellow dots show the locations where maximum wind speed exceeds 33 m s^{-1} along each track.

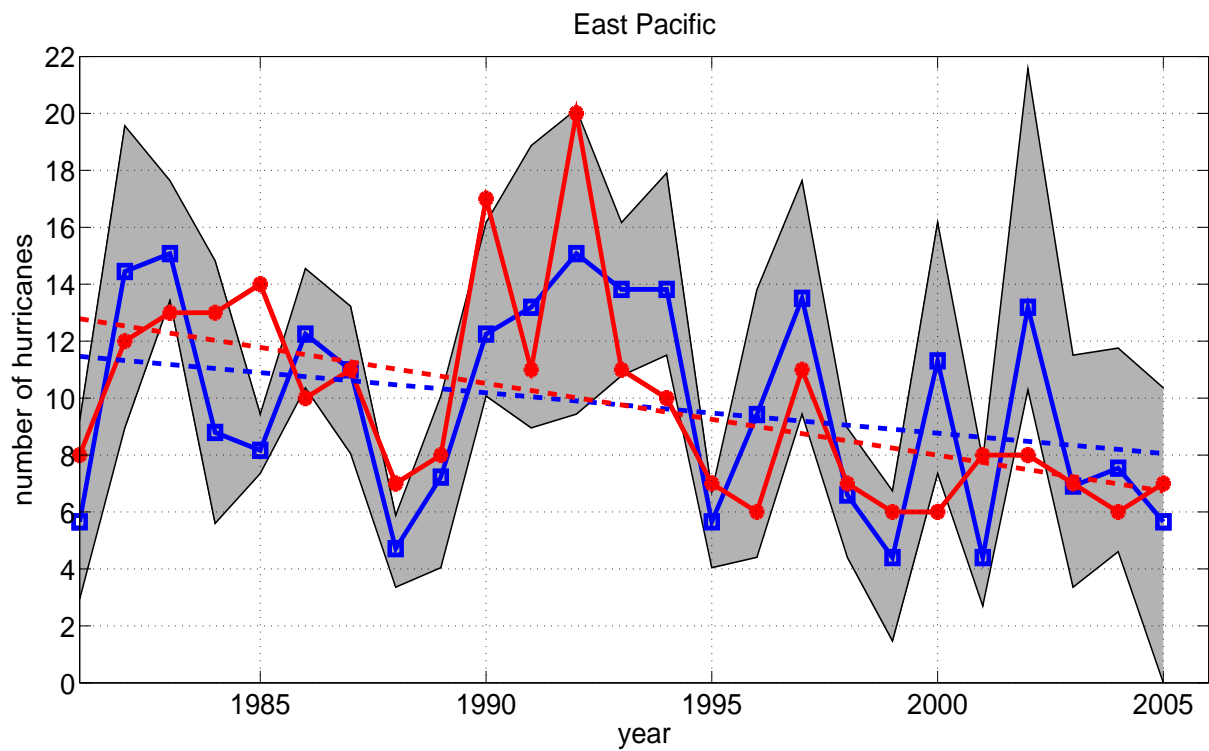


Figure 9. As in Fig. 7 except for the East Pacific.

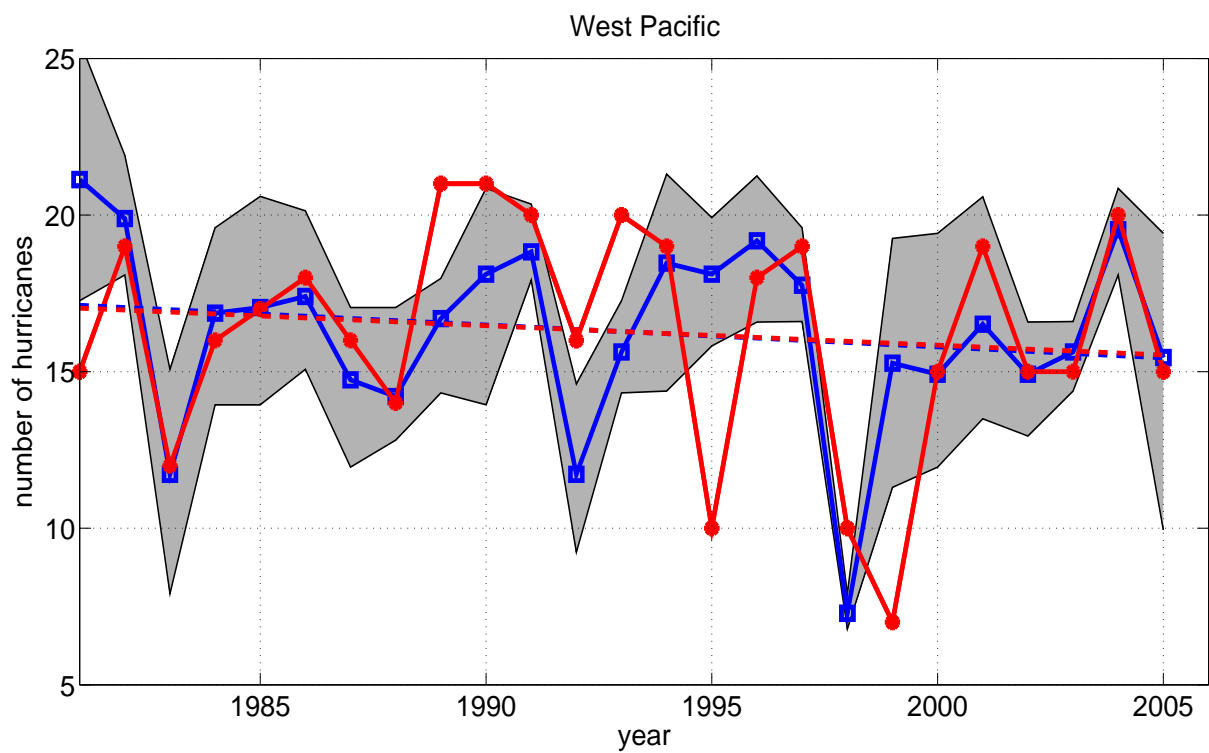


Figure 10. As in Fig. 7 except for the West Pacific.

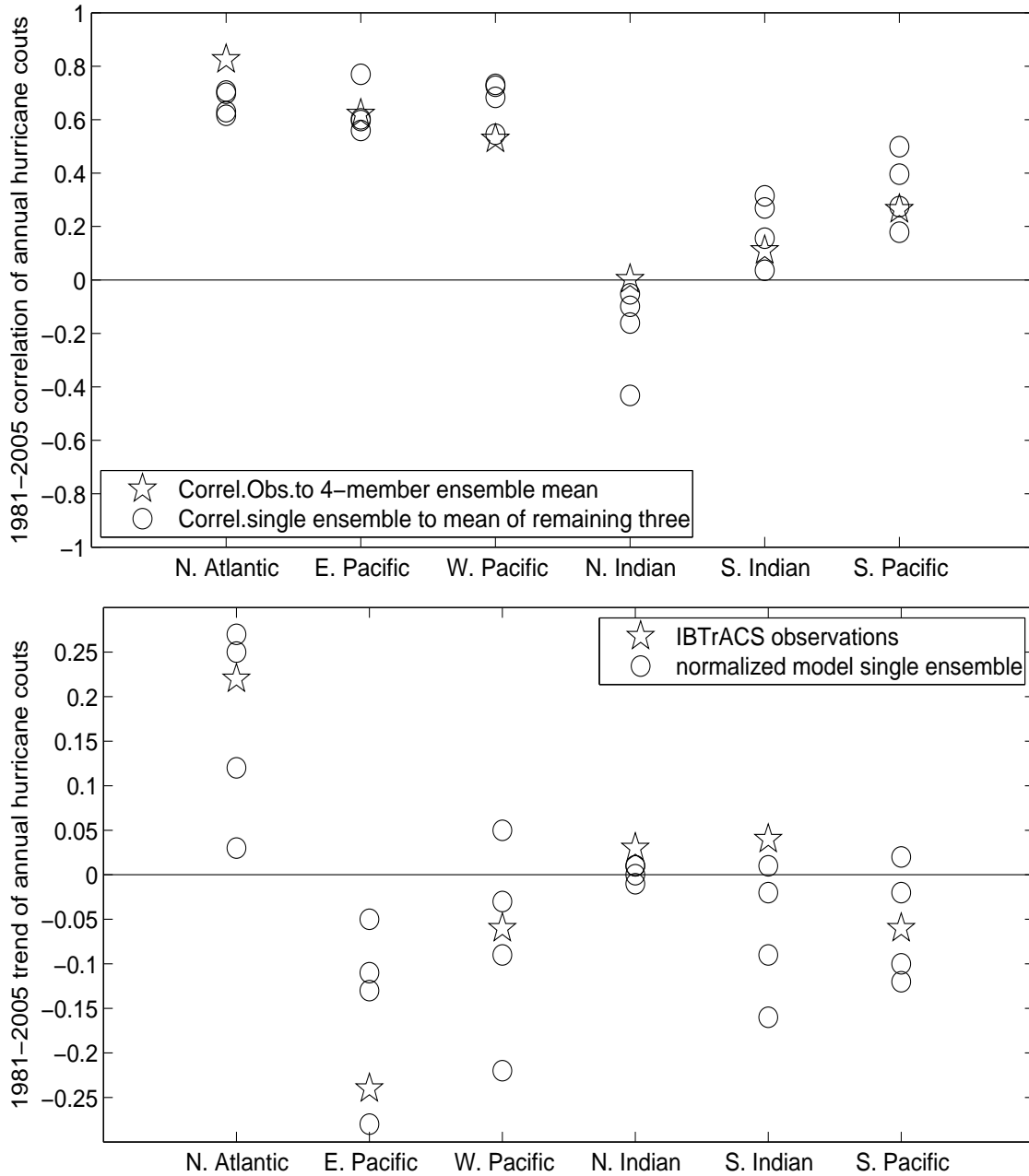


Figure 11. Upper panel: the correlation of observed hurricane count to the 4-member ensemble mean (stars) and the correlation of each ensemble member to the ensemble mean of the remaining three (circles) for each basin. Lower panel: observed (stars) and modeled (circles) linear trends in hurricane frequency for the period 1981-2005 in each basin. Model trends are from individual realizations and calculated from normalized time series.

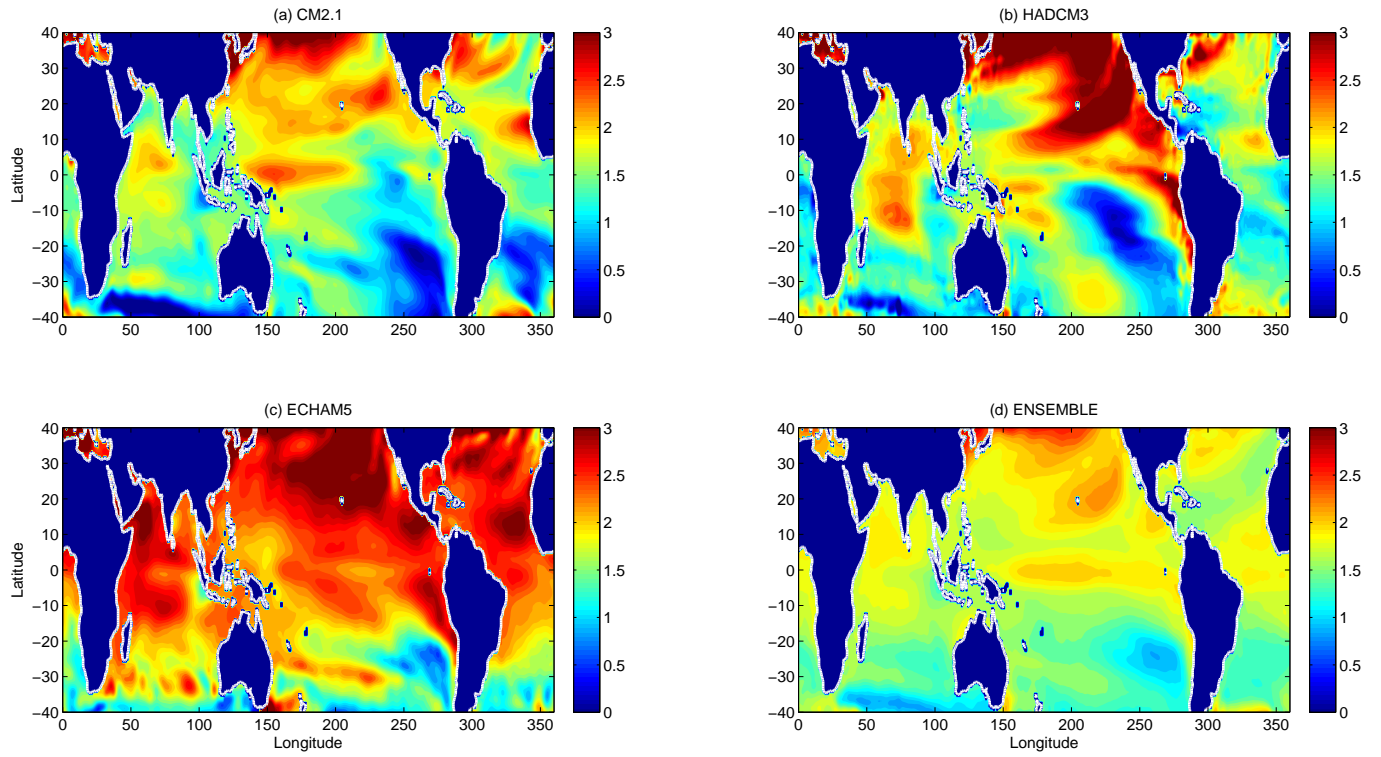


Figure 12. Aug-Sept-Oct seasonal mean SST anomaly from a) GFDL CM2.1, b) UKMO HADCM3, c) MPI ECHAM5 and d) multi-model ensemble mean (see detailed description in the text). Unit: $^{\circ}\text{K}$.

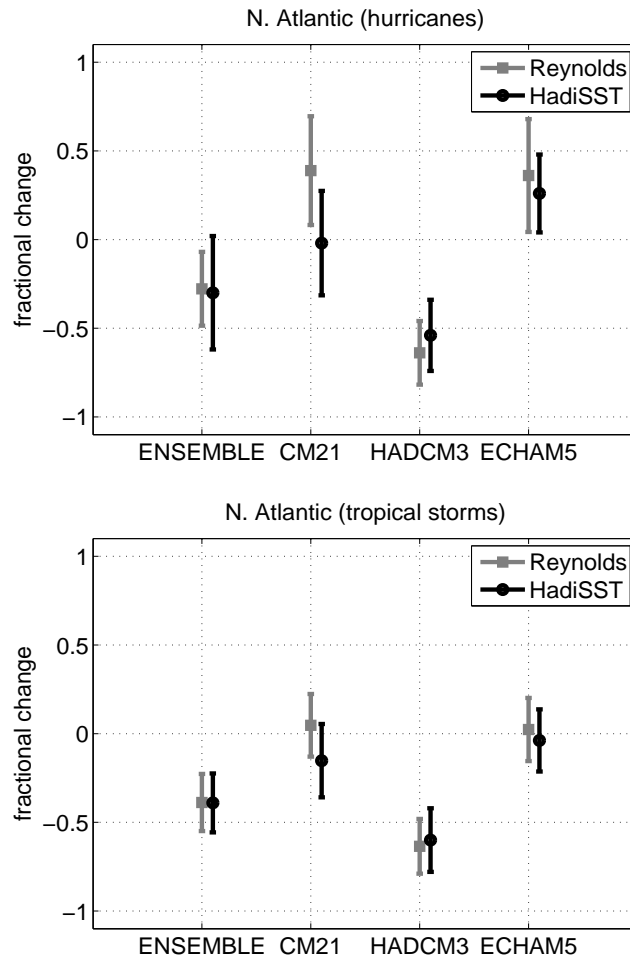


Figure 13. Fractional changes in annual hurricane (upper) and tropical storm (lower) count for the North Atlantic basin from the 4 SST anomaly simulations based on 2 different control climatological-SSTs. Error bars show the 90% confidence level assuming the sampling distributions are normally distributed. Legend shows the two control climatological-SSTs.

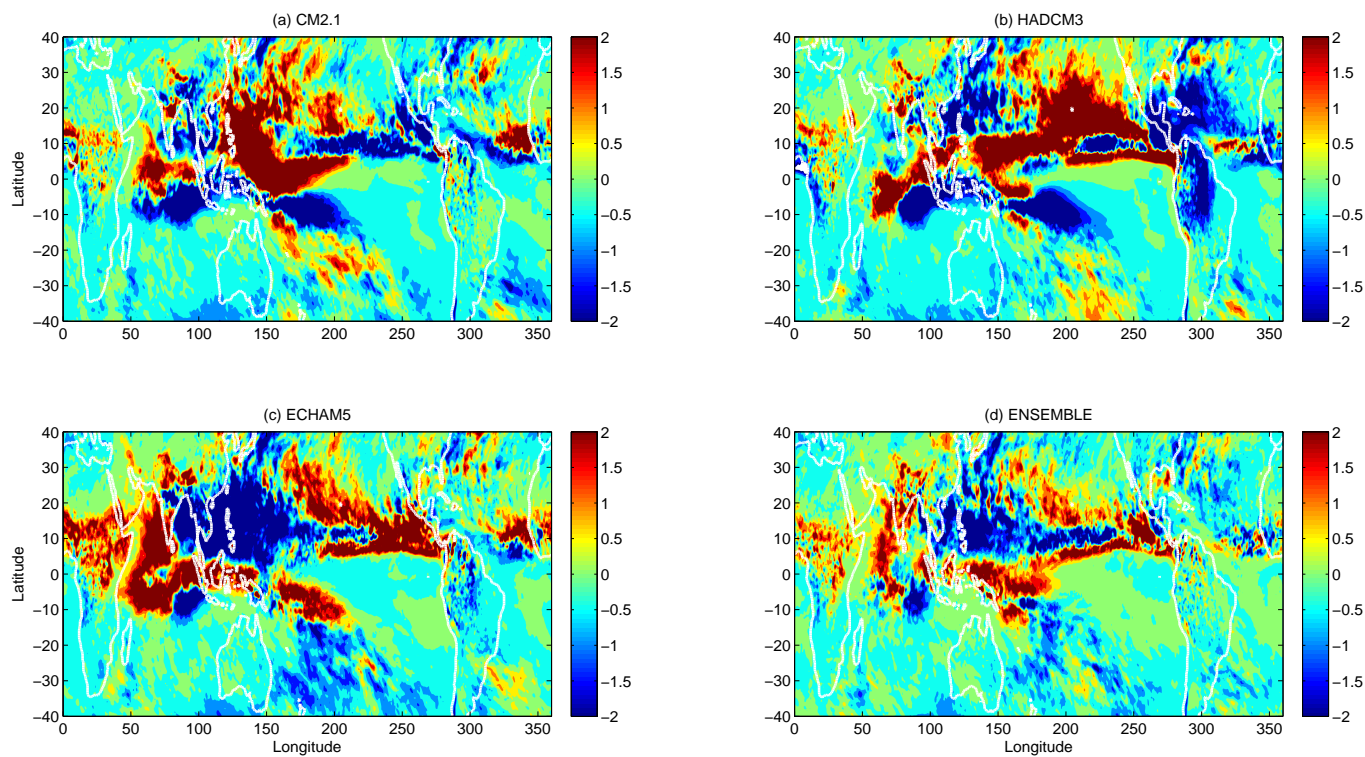


Figure 14. Aug-Sept-Oct seasonal mean precipitation differences between SST anomaly simulations and the control simulation. Unit: mm day^{-1} .

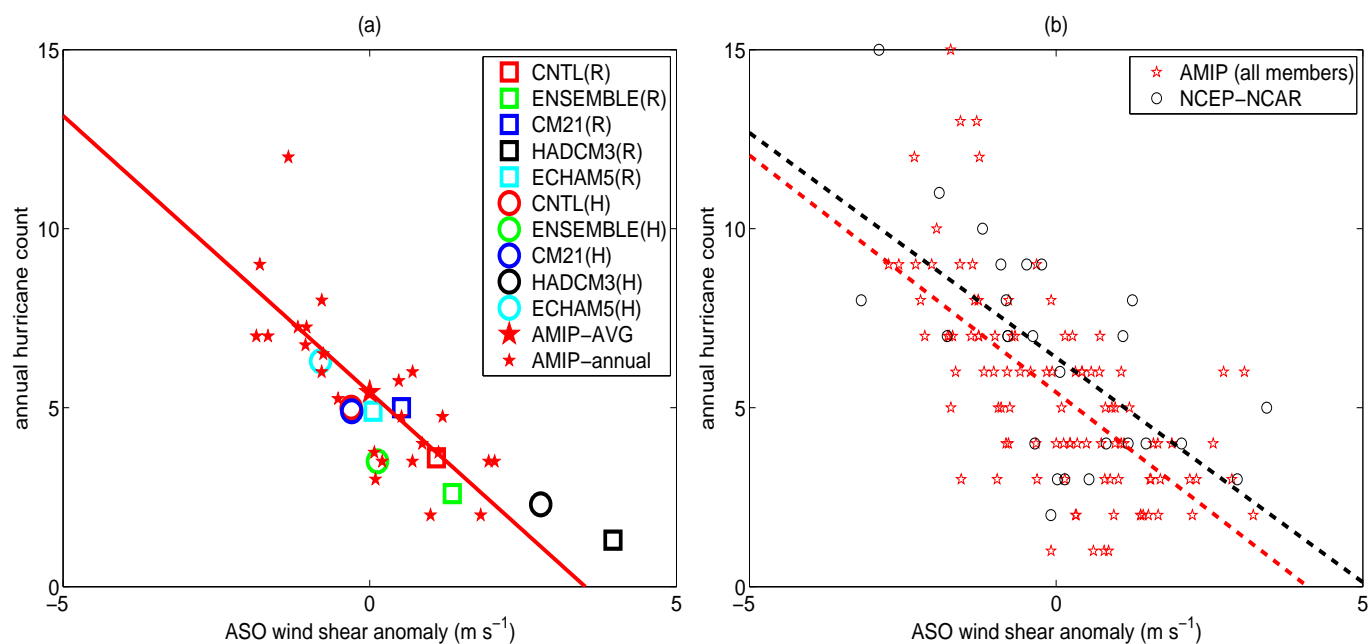


Figure 15. a) Scatter plot of annual Atlantic hurricane count versus ASO season vertical wind shear anomalies from the ensemble mean for each year of the 4 observed-SST simulations (small pentagrams). The big pentagram shows the AMIP all-year mean and the line is a linear regression of the 25 year data points. Also shown are results from the two control climatological-SST simulations (red symbols) and the various SST anomaly simulations (green: ENSEMBLE, blue: CM2.1, black: HADCM3, cyan: ECHAM5). Squares denote the set of experiments using Reynolds climatological-SST as a control, circles denote the set of experiments using HadISST climatological-SST as a control. For the control and SST anomaly simulations, the ASO wind shear anomalies are the mean ASO wind shear minus the AMIP all-year mean. b) As in a) except showing all members of the AMIP runs with all climate change experiments removed. Black circles show scatter plots of observed Atlantic hurricane count versus vertical wind shear calculated from NCEP-NCAR reanalysis. The red and black lines are respectively linear regression of the model and observation data points.

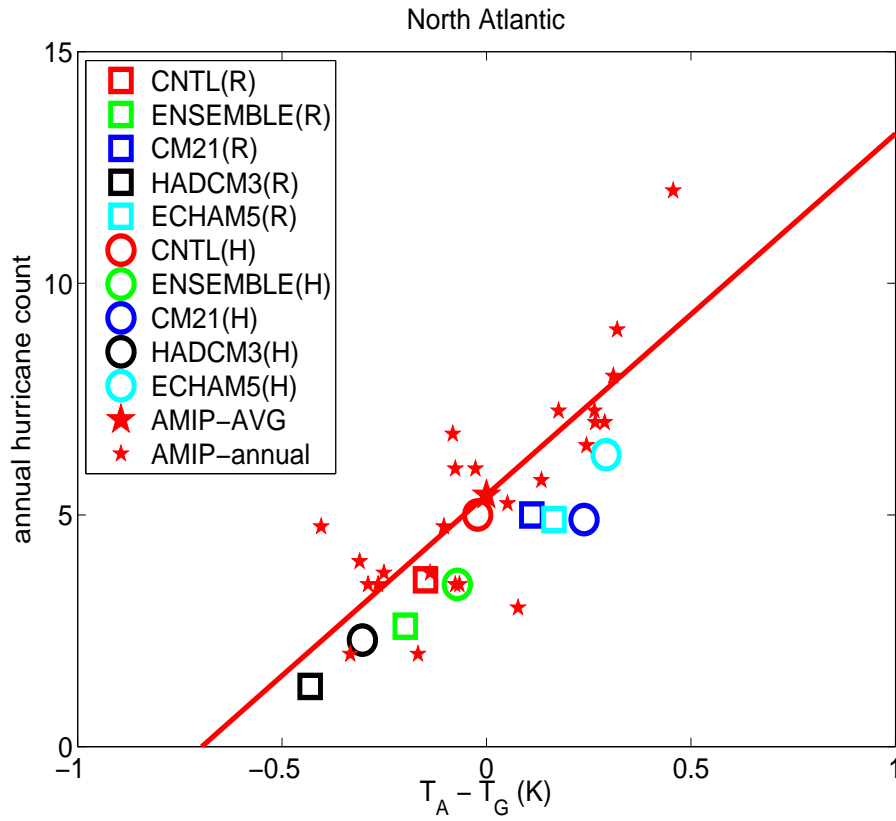


Figure 16. As in Fig. 15a except for scatter plot of annual Atlantic hurricane count versus ASO season Atlantic MDR SST (T_A) minus tropical mean SST (T_G); $T_A - T_G$ is shown as anomalies from the climatological value obtained for the period of 1981-2005.

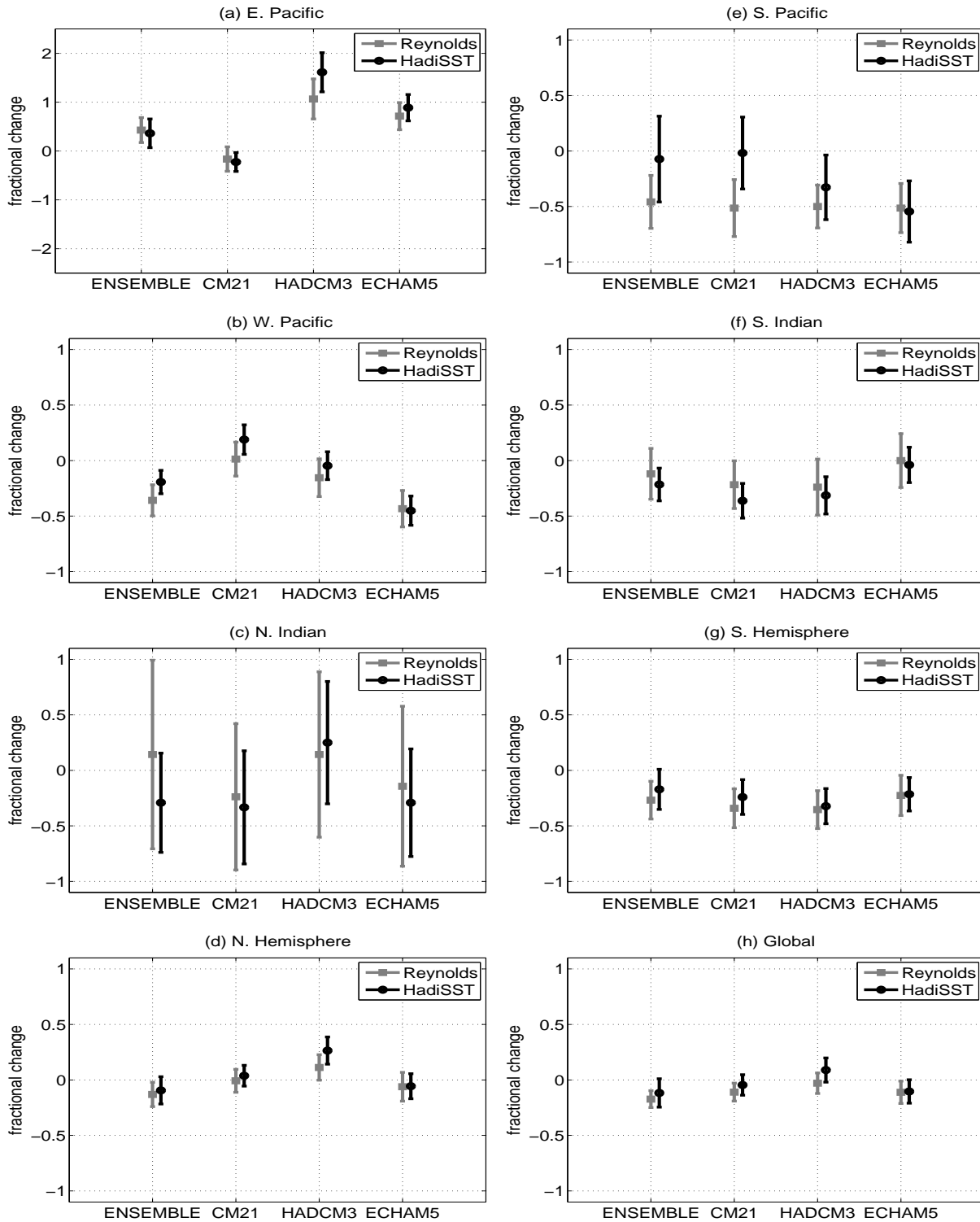


Figure 17. Fractional changes in annual hurricane counts (as in Fig 13a) except for a) East Pacific, b) West Pacific c) North Indian, d) Northern Hemisphere, e) South Pacific, f) South Indian, g) Southern Hemisphere, and h) the global ocean. Error bars show the 90% confidence level assuming the sampling distributions are normally distributed.

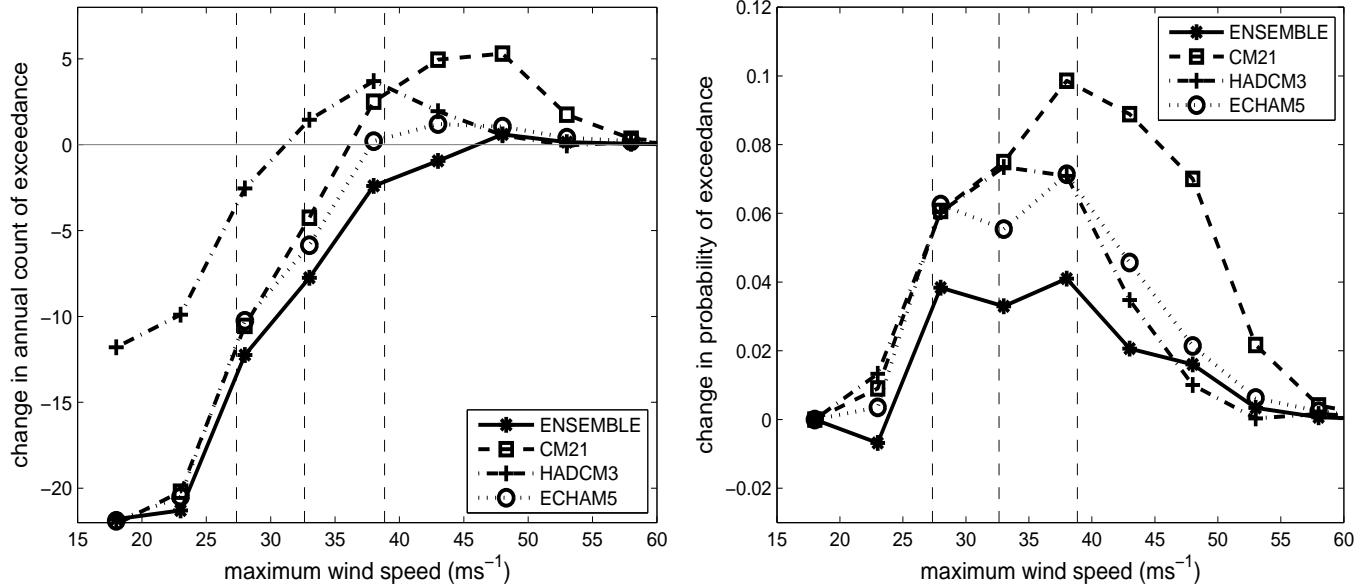


Figure 18. a) Change (warming minus control) in annual storm count exceeding a given surface maximum wind for the entire global tropical ocean. Vertical lines show the lower quartile, median, and upper quartile of the controls. b) As in a) but show change in the probability of exceedance of tropical storm intensity. Positive value indicates relative increase in the fraction of storms with maximum surface wind speed above the corresponding value.